The Pennsylvania State University

The Graduate School

Department of Mechanical and Nuclear Engineering

ANISOTROPIC HEAT CONDUCTION EFFECTS IN PROTON EXCHANGE MEMBRANE FUEL CELLS

A Dissertation in

Mechanical Engineering

by

Chaitanya Jayant Bapat

Submitted in Partial Fulfillment
of the Requirements
for the Degree of

Doctor of Philosophy

December 2008

The thesis of Chaitanya Jayant Bapat was reviewed and approved* by the following:

Stefan Thynell
Professor of Mechanical Engineering
Thesis Advisor
Chair of Committee

Fan-Bill Cheung
Professor of Mechanical & Nuclear Engineering

Panagiotis Michaleris
Associate Professor of Mechanical Engineering

Serguei Lvov
Professor of Energy & Geo-Environmental Engineering

Karen A. Thole
Professor of Mechanical Engineering
Department Head of Mechanical and Nuclear Engineering

*Signatures are on file in the Graduate School

ABSTRACT

Two-dimensional single-phase and two-phase models were used to investigate the behavior of a PEM fuel cell under different steady-state conditions. It was observed that, a high value of the in-plane thermal conductivity for the GDLs is essential for achieving smaller temperature gradients. This was determined to be even more important for thin GDLs. At a given fixed voltage and high humidity inlet conditions, the fuel cell generates maximum current density for bipolar plates with narrow ribs and for GDLs with low through-plane and high in-plane thermal conductivities. It is also predicted that for low humidity operating conditions, the fuel cell generates maximum current density if the GDL is tailored to have high through-plane thermal conductivity and wider ribs near the inlet and progressively decreasing through-plane thermal conductivity and narrower ribs at distances away from the inlet. Additionally, analysis of the effects of anisotropic electrical resistivity shows that, in case of GDLs with high anisotropic thermal conductivity, the maximum and minimum temperatures in a cathode catalyst layer correlate with the average current density and not the local current density.

A three-dimensional model was also developed to analyze external heating techniques used for PEMFC startup. The analysis shows that the thermal mass of the bipolar plates is an important factor affecting the startup time. Therefore, thin, flexible, planer electric heaters are better suited for PEMFC heating applications than the cartridge heaters. Also, GDLs with low through-plane thermal conductivities and high in-plane thermal conductivities are able to reduce the startup time when used in conjunction with a heating element embedded within the GDL.

TABLE OF CONTENTS

LIST OF FIGURES

LIST OF TABLES

NOMENCLATURE

A_{lg}	Gas-liquid interfacial area per unit volume (m^{-1})
A	Active area (m^2), Area of cross-section of wire (m^2)
A_{cross}	Area of cross-section of the channel (m^2)
a	Water vapor activity
C	Molar concentration (mole m^{-3})
c	Specific heat capacity (kJ $kg^{-1}K^{-1}$)
D	Diffusivity (m^2s^{-1})
d	Diameter (m)
d_{hyd}	Hydraulic diameter (m)
EW	Equivalent weight (kg $equiv^{-1}$)
F	Faradays constant (C $mole^{-1}$)
GDL	Gas diffusion layer
h	Convective heat transfer coefficient (W m^{-2} K^{-1})
$h_{contact}$	Thermal contact conductance (W/m^2K) $h_{contact} = \frac{q''_{\text{interface}}}{\Delta T_{\text{interface}}}$
i, i	Local onic current density (A m^{-2})
i_{tot}	Total current density produced by the fuel cell (A m^{-2})
i_o^{ref}	Reference current density (A m^{-3})
J	Volumetric source term (kg $m^{-3}s^{-1}$)
j	Volumetric electrochemical reaction rate (A m^{-3})
K_H	Henry's law constant (Pa-m^3 $moles^{-1}$)

K_p	Hydraulic permeability (m^2)
K_{gr}	Relative permeability for gas phase
K_{lr}	Relative permeability for liquid phase
k	Thermal conductivity (W m^{-1} K^{-1})
k_f	Thermal conductivity of fluid (W m^{-1} K^{-1})
k_{xx}	Through-plane thermal conductivity (W m^{-1} K^{-1})
k_{yy}	In-plane thermal conductivity (W m^{-1} K^{-1})
L_x	Thickness of GDL (m)
L_{y1}	Half width of gas channel (m)
L_{y2}	Half width of current collector (m)
L_w	Latent heat of vaporization of water (J/kg)
l	Length of wire (m)
MEA	Membrane Electrode Assembly
m	Mass (kg)
Nu	Nusselt number
n_{oe}	Electro-osmotic drag coefficient
P	Perimeter of cross-section. (m)
PEM	Proton Exchange Membrane
p	Pressure (Pa)
q'''	Heat source (W/m^3)
R	Universal gas constant (J $mole^{-1}K^{-1}$), Electric resistance (Ohm)

R_{gc}	Thermal resistance to flow to gas channel (K/W)
R_{cc}	Thermal resistance to flow to current collector (K/W)
$R_{c\text{-}cc}$	Non-dimensional thermal resistance
Re	Reynolds number
S	Volumetric source term (mole $m^{-3}s^{-1}$)
T	Temperature (K)
t	Time (s)
U_o	Open circuit potential (V)
V_{cell}	Cell voltage (V)
V_o	Molar specific volume of water (m^3 $mole^{-1}$)
ΔV_{net}	total volume of all the computational cells adjacent to the GDL/bipolar plate interface
$\mathbf{v}$	Velocity (m s^{-1})
W	Heat supplied (W)

Greek letters

α	Phase volume fraction
α_a	Anodic transfer coefficient
α_c	Cathodic transfer coefficient
γ_{lg}	Interphase molar transfer coefficient (m s^{-1})
ε	Porosity
θ	Contact angle (°)

κ	Membrane ionic conductivity (S m^{-1})
μ	Viscosity (Pa-s)
ρ	Density (kg m^{-3})
$\boldsymbol{\sigma}, \sigma$	Surface tension (N m^{-1}) , Electrical resistivity (Ω m)
$\boldsymbol{\tau}$	Viscous stress (Pa)
ϕ	Potential (V)

Superscripts

i	Component

Subscripts

a	Anode
c	Capillary, Cathode
eq	Equivalent
g	Gas
yy	In-plane
l	Liquid
m	Membrane
p	Constant pressure
por	Porous material
xx	Through-plane
wp	Wetting phase

ACKNOWLEDGEMENTS

I would like to thank Dr. S. T. Thynell for his excellent guidance and support throughout my graduate studies. I would like to acknowledge the financial support provided by National Science Foundation for this project. I would also like to thank my doctoral committee members Dr. Fan-Bill Cheung, Dr. P. Michaleris and Dr. Serguei Lvov for their time and guidance.

I would like to thank Jen and LaTrisha for all their help. Finally, I would like to thank all my friends who have made my stay at Penn State wonderful and worth remembering.

Chapter 1

Introduction

1.1 Overview

Fuel cells are electrochemical devices that convert chemical energy directly into electricity. The theoretical efficiency of a fuel cell is given by [1],

$$\xi_{th} = 1 - \frac{T\Delta S}{\Delta H} \tag{1.1}$$

At temperatures below 200°C, the theoretical efficiencies of fuel cells are much higher than the efficiency of the Carnot cycle. In fact, for certain fuel cells like the formic acid/oxygen fuel cell, the theoretical efficiency is greater than 100% because the ΔS for the complete combustion of these fuels is a positive number. Thus, fuel cells have the potential to produce power efficiently at lower temperatures. Over the past decade, there has been an increasing amount of interest in the use of proton-exchange-membrane (PEM) fuel cells as an environmentally friendly power source. In these cells, oxygen and hydrogen combine to form water, and a part of the chemical energy is directly converted to electricity. Thus the PEMFC produces no harmful emissions. It also operates at much lower temperatures than conventional internal combustion engines and is also thermodynamically more efficient. It is envisaged that these cells would start replacing internal combustion engines towards the end of the current decade. This would require the development of a large-scale hydrogen infrastructure [2], and a cell that would be able to produce power at adequate power density and at good energy conversion

efficiency [3]. A better understanding of the various processes affecting the operation of a PEMFC is required to develop this cell as a viable option for the future.

A PEMFC consists of a polymer electrolyte with catalyst layers sandwiched between two gas-diffusion electrodes. The reactant gases flow through the gas channels made into the current collector plate also known as the bipolar plate. The reactant gases are hydrogen at anode and air at cathode for a PEMFC. The gases then diffuse through the porous gas-diffusion layers and react at the catalyst layers which are a mixture of fine platinum particles and membrane supported on relatively large carbon particles. The overall chemical reaction is given by:

$$2H_2 \longrightarrow 4H^+ + 4e^- \qquad \text{anode}$$

$$O_2 + 4H^+ + 4e^- \longrightarrow 2H_2O \qquad \text{cathode}$$

The protons diffuse through the polymer electrolyte membrane, whereas the electrons are conducted through the current collector plates to an external circuit. It should be noted that one or two water molecules are also transported across the membrane with the proton [4]. Coolant water is circulated through the channels machined into the coolant plate to remove excess heat. A schematic of a typical PEMFC is shown in Fig. 1.1.

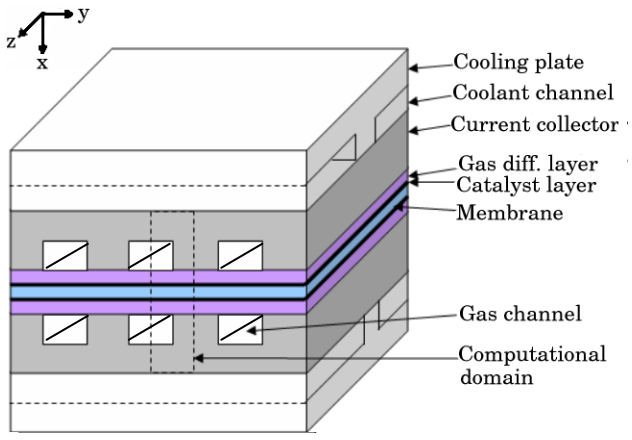

Fig. 1.1. Schematic of PEM fuel cell.

It is desirable to control the various parameters affecting fuel-cell operation in a manner that allows stable operation over long periods of time. In the present work we develop a numerical model for fuel-cell operation and analyze the effects of different parameters which have been neglected in previous studies. In particular, we analyze the effect of anisotropic thermal conductivity of the GDLs on the polarization and startup behavior of a fuel cell. Such an analysis is expected to reveal the criteria for tailoring the thermal conductivities of the GDLs to improve the electrical output of a fuel cell.

We begin analysis in chapter two where we use a two-dimensional single-phase model to analyze the effect of an anisotropic thermal conductivity of GDLs and membrane on temperature distribution in a fuel cell. In chapter three we extend our analysis to include two-phase effects and study the effect of anisotropic thermal conductivity of the GDLs on current density and membrane dehydration. We also develop a methodology to optimize the thermal conductivity of GDLs and dimensions of bipolar plates to maximize the current density at low humidity operating conditions. We further extend our model to include the effects of anisotropic electrical conductivity in chapter four. In chapter five, we use a three dimensional single-phase model to analyze the effectiveness of different external heating techniques for rapid startup of a fuel cell. A brief summary of all the results is presented in the last chapter.

1.2 References

[1] Veilstich, W., 2003, *Handbook of Fuel Cells – Fundamentals, Technology and Applications, Volume 1: Fundamentals and Survey of systems*, John Wiley & Sons, Ltd., Chichester, England, 2003, pp. 26.

[1] Feng, W., Wang, S., Weidou, N., and Chen, C., 2004, *Int. J. Hydrogen Energy*, vol. 29, p. 355.

[2] Ahluwalia, R. K., Wang, X., Rousseau, A., and Kumar, R., 2004, *J. Power Sources*, vol. 130, p. 192.

[3] Choi, K. H., Peck, D. H, Kim, C. S., Shin, D. R., and Lee, T. H., 2000, *J. Power Sources*, vol. 86, p. 197-201.

Chapter 2

Effect on temperature distribution

As a preliminary step towards the development of a more representative and complete model, a single-phase model with a primary focus on heat transfer inside the fuel cell was developed and implemented to assess the importance of various parameters on the temperature distribution inside the cell.

2.1 Introduction

Many modeling efforts have been made to study the electrochemical-thermal aspects of fuel cells. The initial efforts in this field were made by Springer [1] and Bernardi and Verbrugge [2,3], who developed one-dimensional isothermal models for studying the effects of mass diffusion and species transport through the porous electrodes and membrane. The earliest attempts to model water and heat management issues in a PEM fuel cell were made by Fuller and Newman [4] and by Nguyen and White [5]. Djilali and Lu [6] developed a one-dimensional, non-isothermal model for studying the performance at different current densities. Wohr and coworkers [7,8] and Rowe and Li [9] also developed one-dimensional non-isothermal models to study the effects of various other parameters on fuel-cell operation. Dutta et al. [10] developed a three-dimensional single-phase isothermal model for studying transport processes in a fuel cell. Wang et al. [11,12] also developed a multi-dimensional isothermal model for simulating transport

processes in a fuel cell with liquid water confined to catalyst layers. They analyzed the effects of hydrogen dilution at the anode inlet and inter-digitated flow field on the performance of the fuel cell. Berning et al. [13] and Zhou and Liu [14] also developed three-dimensional non-isothermal models for studying fuel-cell behavior. Ju et al. [15] developed a three-dimensional single-phase non-isothermal model to study the effects of variation of thermal conductivity of the GDL and inlet humidity on fuel-cell operation. Sivertsen and Djilali [16] also developed a non-isothermal three-dimensional model for simulating fuel-cell operation and integrated it with a commercial CFD software. All these models neglected the effects of water-vapor condensation on cell performance. Baschuk and Li [17] formulated a model to predict the performance of a fuel cell in the diffusion limited region of the polarization curve (high current densities). However, their model did not have an explicit two-phase model to predict the flow of different phases. Stockie [18] developed a two-dimensional model by taking into account the effects of phase and temperature change in a fuel-cell cathode. Berning and Djilali [19] developed a two-phase, multi-dimensional, non-isothermal model for fuel-cell simulation based on the unsaturated flow theory [20]. Wang et al. [21] developed a two-phase model for simulating transport processes in a fuel-cell cathode based on the multi-phase mixture model developed by Wang and Cheng [22]. Hu et al. [23,24], Mazumder and Cole [25] and Sun et al. [26] also developed models based on the multiphase mixture model. Birgersson et al. [27] developed a two-phase, non-isothermal model for a PEMFC. Shimpalee et al. [28] implemented their two-phase model on a high performance cluster to simulate a large-scale PEMFC. Recently, Baschuk and Li [29] developed a three-dimensional formulation for modeling fuel-cell transport processes based on a two-phase,

two-fluid porous media model which incorporated a spatial temperature variation. However, a complete three-dimensional implementation of this model has not yet been made.

Apart from the above models, there have been studies which concentrated on certain other specific aspects of fuel-cell operation. Nam and Kaviany [30] studied the effects of water saturation and two-layer GDL on fuel-cell operation using a one-dimensional non-isothermal model. Pasaogullari and Wang [31,32] studied the role of a micro-porous layer in the cathode GDL on the phase distribution. Yuan and coworkers [33] studied the variation in temperature of reactant gases in both cathode and anode gas channels. Musser and Wang [34] studied the variation of coolant temperature through the length of the cooling channel for different operating conditions of the cell. Mawardi et al. [35] studied the optimization of operating parameters of a fuel cell for obtaining the best performance. However, none of the above mentioned works considered the possible effects of anisotropic thermal conductivity of GDLs and membrane on operation of the fuel cell.

It is known that the GDLs and the polymer electrolyte membrane are fibrous polymer-like materials. Kurabayashi [36] noted that thin polymer films tend to show anisotropic behavior in their thermal diffusivity, as the energy transport is more efficient along the polymer chains. This has also been confirmed by many previous and new experimental results [37-39]. The ratio of conductivities in directions parallel and perpendicular to the polymer chain can also be very high. In case of GDLs and membrane, such preferential alignment of fibers or polymeric chains can lead to an anisotropic thermal conductivity. The thermal contact conductance at the interfaces of

different layers in the fuel cell is also expected to have a significant effect on the temperature distribution inside the cell. The purpose of this paper is to bring out the effect of anisotropic thermal conductivity and thermal contact conductance on the temperature distribution within the fuel cell using a single-phase, two-dimensional model.

2.2 Model formulation

The PEMFC generates in some cases almost 50% of waste heat of the total available energy. This heat has to be effectively dissipated for stable and reliable operation of the fuel cell. The heat generated is caused by 1) kinetic loss in the catalyst layers (largely cathode), 2) ohmic loss in the membrane and catalyst layers, and 3) reversible heat release. In the present work, a single-phase, two-dimensional model is used to assess the effects of anisotropic thermal conductivity and thermal contact resistance on the overall temperature distribution inside the cell. The complete model consists of coupled flow, species, electrochemistry and heat transport models. The two-dimensional computational domain chosen for the present work is shown in Fig. 1.1.

2.2.1 Flow model

The single-phase mass and momentum balance equations with appropriate source terms for the porous drag, production/consumption of reactants and the electro-osmotic drag in the membrane are solved all over the domain. The mass and momentum balances are, respectively, written as:

$$\frac{\partial \varepsilon \rho}{\partial t} + \nabla \cdot (\varepsilon \rho \mathbf{v}) = -\nabla \cdot \left(\frac{n_{oe} M_{H_2O}}{F} \mathbf{i} \right) + J \tag{2.1}$$

and

$$\frac{\partial}{\partial t}(\varepsilon \rho \mathbf{v}) + \nabla \cdot (\varepsilon \rho \mathbf{v}\mathbf{v}) = -\nabla(\varepsilon p) + \nabla \cdot (\varepsilon \boldsymbol{\tau}) - \frac{\mu}{K_p} \mathbf{v} \tag{2.2}$$

Here the first term on the right hand side of Eq. (2.1) represents the source term due to the electro-osmotic drag, and the last term represents the source due to production/consumption of reactants and products. This source term is

$$J = -\frac{| FS^{H^+} |}{2F} M_{H_2} \tag{2.3}$$

for the consumption of hydrogen in anode catalyst layer, whereas

$$J = -\frac{| FS^{H^+} |}{4F} M_{O_2} \tag{2.4}$$

$$J = \frac{| FS^{H^+} |}{2F} M_{H_2O} \tag{2.5}$$

are used to describe the consumption of oxygen and production of water, respectively, in the cathode catalyst layer. In addition, the last term in Eq. (2.2) represents the source term due to porous drag and is based on Darcy's law.

2.2.2 Species transport model

The flow of reacting species (hydrogen and oxygen) and water vapor is modeled by solving the species conservation equation for each of these species. The species conservation equation for species *i* is given by:

$$\frac{\partial}{\partial t}\left(\varepsilon C^i\right)+\nabla\cdot\left(\varepsilon \mathbf{v} C^i\right)=\nabla\cdot\left(\varepsilon D^i \nabla C^i\right)+S^i \tag{2.6}$$

The source terms for this equation (S^i) are the same as those given by Eqs. (2.3)-(2.5), except they are molar-based quantities.

2.2.3 Electrochemical reactions

The electrochemistry is included by solving conservation of membrane phase potential over the membrane electrode assembly (MEA) with appropriate source terms in the catalyst layers for the production and consumption of protons by electrochemical reactions:

$$-\nabla\cdot\left(\kappa\nabla\phi_m\right)=FS^{H^+} \tag{2.7}$$

The solid phase (the platinum-carbon matrix) is assumed to be a good electrical conductor and hence the solid-phase potential is assumed to be constant in the catalyst layers.

The electrochemical reactions are modeled using the Butler-Volmer rate expressions [40], and in anode and cathode catalyst layers are, respectively, given by:

$$FS^{H^+}=j_a=i_{oa}^{ref}\left[\exp\left\{\frac{\alpha_a F}{RT}\left(\phi_s-\phi_m\right)\right\}-\exp\left\{-\frac{\alpha_c F}{RT}\left(\phi_s-\phi_m\right)\right\}\right]\left(\frac{C_{H_2}}{C_{H_2}^{ref.}}\right)^{0.5} \tag{2.8a}$$

$$=j_c=i_{oc}^{ref}\left[\exp\left\{\frac{\alpha_a F}{RT}\left(\phi_s-\phi_m\right)\right\}-\exp\left\{-\frac{\alpha_c F}{RT}\left(\phi_s-\phi_m\right)\right\}\right]\left(\frac{C_{O_2}}{C_{O_2}^{ref.}}\right) \tag{2.8b}$$

and elsewhere

$$FS^{H^+}=0 \tag{2.8c}$$

2.2.4 Heat transport model

The flow rates of gases inside the GDLs are expected to be extremely small due to the presence of the porous medium. Hence, heat transfer due to the flow of these gases is neglected. The heat flow is modeled using the two-dimensional heat conduction equation given by

$$\frac{\partial}{\partial t}(\rho c T) = k_{xx}\frac{\partial^2 T}{\partial x^2} + k_{yy}\frac{\partial^2 T}{\partial y^2} + q''' \tag{2.9}$$

where the transient term is included in the numerical scheme even though only steady state is considered. Here, the heat source terms within the anode catalyst layer, membrane and cathode catalyst layer, are, respectively, given by

$$q''' = \mid j_a(\phi_s - \phi_m)\mid + \frac{i_m^2}{\kappa} \tag{2.10a}$$

$$q''' = \frac{i_m^2}{\kappa} \tag{2.10b}$$

$$q''' = \mid j_c(\phi_s - \phi_m)\mid + \frac{i_m^2}{\kappa} + \mid T\Delta S\frac{j_a}{2F}\mid - \frac{\mid FS^{H^+}\mid}{2F}M_{H_2O}L_w \tag{2.10c}$$

The first term for both the anode and cathode source terms corresponds to heat generation due to kinetic loss at the catalyst reactant layer. The next term in both cases represents heat generation due to flow of ions through the membrane material. The membrane source term corresponds to heat generated due to resistance offered to the flow of protons through the membrane. The third term in case of the cathode corresponds to the heat generation due to reversible heat release. The entire reversible heat release due to the chemical reaction is assumed to occur at the cathode [15]. The last term for the

cathode catalyst layer represents enthalpy change due to evaporation. The liquid water generated in the cathode is assumed to instantaneously evaporate to vapor phase. It is also assumed that water vapor can exist in a supersaturated state and behaves like an ideal gas.

2.2.5 Boundary conditions

2.2.5.1 Flow and species transport

The channel pressures and concentrations of reactants and products on the anode and cathode sides are specified as boundary conditions. The experimental result used for validation of this model (see next section) is the polarization curve for the entire fuel cell. Hence it is desirable to use average values of pressures, reactant and product concentrations in order to validate the results. The average model parameters are calculated using an approximate analysis.

The densities of the reactant gas mixtures are calculated at exit conditions and are assumed to be constant. The temperature change of the reactant gases is neglected. The pressure variation is calculated using Bernoulli's equation with an additional term to account for the effect of wall friction. The exit concentrations are calculated using simple mass balances accounting for the production/consumption of reactants. The average quantities are taken as the arithmetic means of the inlet and outlet quantities. In spite of these simplifications, the above method of calculating the average parameters takes into account the effect of reactant flow rates, channel length and active area, which otherwise cannot be accounted for in a two-dimensional model. It is noticed that the average values

calculated above depend on the current, which is obtained from the solution of the electrochemistry model. Hence these boundary conditions are also updated during each iteration of the numerical scheme.

2.2.5.2 Electrochemistry

In this chapter, we study the effect of thermal contact conductance at the GDL/current collector interface and anisotropic thermal conductivity on the temperature distribution inside the cell. It is expected that as the thermal contact conductance changes, the electrical contact resistance at that interface will also change. In the current model the electrochemical equations are solved over the MEA. Hence the effect of electrical contact resistance is taken into account in the boundary conditions. At the GDL/anode interface, they are

$$\phi_s = U_0 - V_{cell} - iAR_{acontact} - iAR_{gdl} \tag{2.11a}$$

$$\nabla \phi_m = 0 \tag{2.11b}$$

At the GDL/cathode interface, they are

$$\phi_s = iAR_{ccontact} + iAR_{gdl} \tag{2.12a}$$

$$\nabla \phi_m = 0 \tag{2.12b}$$

The corresponding heat generation terms are also added to the heat transport equation (Eq. 2.9). Again the analysis presented above is simplified and more complicated issues involving the anisotropic electrical conductivity of the GDLs have not been addressed. It should also be noted that the above boundary conditions are dependent

on the electric current which comes out of the solution of the electrochemical equations. Hence, they are also updated during each iteration of the numerical scheme, as in case of the flow boundary conditions.

2.2.5.3 Heat transfer boundary conditions

The symmetrical sections through the gas channels and bipolar plates are assumed to be insulated (symmetry boundary condition). Characteristic *Re* numbers for flow in the gas channels are low and in the laminar range. Hence, the heat transfer coefficients for the gas and coolant channel were calculated using [41]

$$Nu = 2.98 \tag{2.13}$$

since entry lengths are relatively short compared to channel lengths. Additionally, the channel boundaries are at nearly a uniform temperature. The effect of a variable temperature along the GDL boundary on the overall heat transfer coefficient is neglected. The gas channels were assumed to have a square cross-section. The gas and coolant temperatures were assumed to be at 343K (cell operating temperature).

2.2.6 Property values

2.2.6.1 Ionic conductivity

The ionic conductivity of the membrane is computed from the correlation given by [1]

$$\kappa = (0.5139\lambda - 0.326)\exp\left[1268\left(\frac{1}{303} - \frac{1}{T}\right)\right] \tag{2.14}$$

where

$$\lambda = 0.043 + 17.81a - 39.85a^2 + 36.0a^3 \tag{2.15}$$

2.2.6.2 Cathode exchange current density

The temperature dependence of the cathode exchange current density is evaluated from the correlation given by [42]

$$i_{oc}(T) = i_{oc}^{ref}(353K)\exp\left[-\frac{\Delta E}{R}\left(\frac{1}{T} - \frac{1}{353.15}\right)\right] \tag{2.16}$$

2.2.6.3 GDL/current collector thermal contact conductance

There appears to be no experimental data available in the literature for the thermal contact conductance. Mirmira et al. [43], Marotta and Fletcher [44] and Fuller and Marotta [45] have measured thermal contact conductance values for certain metal-polymer joints. The thermal contact conductance varied from 100 to 2,000 W/m^{2}K for thicker polymers and from 1000 to 10,000 W/m^{2}K for thin elastomeric gaskets. Our in house measurements of this contact conductance yielded a range from 500 to 10,000 W/m^{2}K, depending on applied pressure [46]. Hence the thermal contact conductance was varied from 500 to 10,000 W/m^{2}K in the current analysis.

2.2.6.4 GDL/current collector electrical contact resistance

Mishra et al. [47] measured the electrical contact resistance at this interface. The electrical contact resistance varied from 2.0 to 4.0 mΩ-cm^2 depending on the applied pressure. As the physical mechanisms controlling the thermal and electrical contact resistances are expected to be the similar, a linear relationship was assumed to exist between the thermal and electrical contact resistances.

This completes the description of the numerical model. It captures the basic features of heat generation and transfer inside the PEM fuel cell. It is used to study the steady-state temperature distributions for different operating conditions.

2.3 Numerical scheme

The above model thus consists of a set of two-dimensional equations for modeling species conservation, electrochemistry, fluid flow and heat conduction inside the cell. The values of various parameters used for the model are given in Table 2.1. The coupled

Table 2.1 Model parameters and properties [48].

Quantity	Value
Gas channel length	7.0E-2 m
Gas channel width (= depth)	10.0E-4 m
Membrane thickness	1.08 E-4 m
Gas-diffusion layer thickness	3.0E-4 m
Catalyst layer thickness	10.0E-6 m
Anode humidification temperature	343K

Anode inlet flowrate	1200 cm^3/min
Cathode humidification temperature	343K
Cathode inlet flow rate	2200 cm^3/min
Coolant water temperature	343K
Gas-diffusion layer electrical resistivity	0.005 ohm-cm
Gas-diffusion layer porosity	0.4
Membrane porosity	0.4
Anode reference exchange current density	1.0E8A/m^3
Cathode reference exchange current density	3.0E3A/m^3
Entropy change ΔS for $H_2 + \frac{1}{2}O_2 \rightarrow H_2O_{(liq.)}$	-162.4 (J/mol K)

set of equations was solved iteratively. The heat conduction equation was solved until the relative error in the overall heat balance was $<10^{-3}$, and the flow equations were solved using the SIMPLER scheme [49] until the mass source was $<10^{-8}$. The iterations were continued until convergence criteria for all the equations were simultaneously met. The computational domain was divided into a Cartesian grid of size 32×10, and grid independence was confirmed by solving the problem on a finer grid. The polarization curve was obtained using the model and the cathode reference exchange current density was used as a fitting parameter. The comparison of model results with published experimental results [48] is shown in Fig. 2.1, and a good agreement with the experimental data is obtained except at high current densities. The disagreement at high current densities can be explained due the fact that the model neglects two-phase effects,

three-dimensional details and also the cell temperature is not maintained constant as in was done in the experiments (the coolant temperature is set equal to the cell temperature).

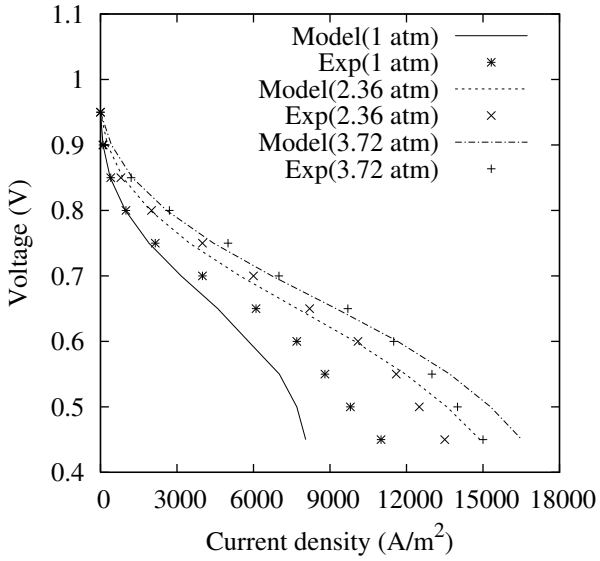

Fig. 2.1 Polarization curve obtained from model and compared with experimental results [48].

The steady-state results obtained using this model for different operating parameter values are presented in the next section.

2.4 Discussion of results

2.4.1 The base case

A parametric study is conducted to examine the effects of various input values on the temperature distribution inside the fuel cell. In order to analyze the effects of various input values, it is important to define reference values against which the variations can be compared. The operating conditions for such a base case are given in Table 2.2. The

Table 2.2 Parameter values for base-case condition.

Parameter	Value
Cell output voltage	0.65 V
Cell operating voltage (Cathode and Anode side)	2.36 atm
Height of the symmetrical section	1.0E-3 m
Channel width : Current collector width	1:1
Isotropic thermal conductivity of membrane and catalyst layers $k_{xx}=k_{yy}$	0.1 W/m-K
Isotropic thermal conductivity of gas-diffusion layers $k_{xx}=k_{yy}$	1.0 W/m-K
Thermal conductivity of air	0.024 W/m-K
Thermal conductivity of water	0.58 W/m-K
Thermal conductivity of current collector (graphite)	85.0 W/m-K
Thermal contact conductance at the diffusion layer / current collector interface	3000 W/m^2K

thermal conductivity for all the reference materials is assumed to be isotropic. The thermal conductivities of the membrane and GDLs are typical values for these materials in a dry state. Any relationship between the electrical and thermal conductivities has been neglected because of the lack of experimental evidence. The current collector plate was assumed to be made of graphite (as in the experiment [48]). Other current collector plates made of materials of different thermal conductivities have not been considered in this study. The thermal contact conductance value at the current collector GDL interface is a typical value for this particular contact (see Sec. 2.2.6.3). The thermal contact conductance at the GDL/catalyst layer interface is not considered due to lack of

experimental data. These operating conditions are typical for a PEMFC. Analysis of this case provides important insights into the thermal behavior of the cell. The temperature distribution for this operating condition is shown in Fig. 2.2. It qualitatively matches the one-dimensional results obtained by Nguyen and White [5] and Rowe and Li [9].

Inspection of Fig. 2.2 reveals that the region in the membrane near the cathode catalyst layer develops relatively high temperatures. This region is susceptible to water loss due to evaporation. Loss of water in the membrane will result in a reduced ionic conductivity and loss of active area. Thus the maximum temperature in the membrane becomes an important output from this study. The region in contact with the current collector tends to be at a lower temperature than the rest of the MEA. Thus this region is susceptible to problems associated with condensation of water vapor. Thus the minimum temperature in the GDLs is also an important output, potentially affecting the operation of the fuel cell. It is also important to determine the difference between these two temperatures. A temperature difference of even 2 to 3K can result a significant difference in the saturation pressure for water. This can lead to vastly different evaporation and condensation characteristics in the vicinity of these two regions. Thus it is important to minimize the temperature gradients inside the cell.

The contact resistance at the interface between the current collector and GDL is expected to play an important role in determining these temperatures. It is also seen that since the current collector also removes excess heat from the MEA, the in-plane thermal conductivity of GDLs is also expected to play an important role in determining the temperature distribution inside the fuel cell. The following sections present the effects of changing various parameters on the temperature distribution inside the cell.

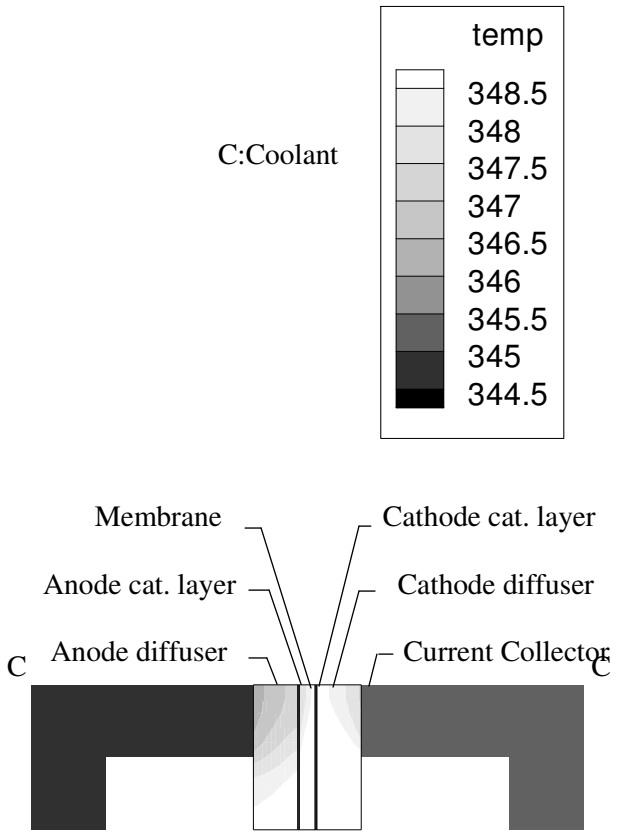

Fig. 2.2 Temperature distribution for base-case operation.

2.4.2 Effect of current density

As discussed previously, many works are available that have assumed the temperature to be uniform. It is important to know the conditions under which such an assumption is reasonable. As the operating current density of the fuel cell increases the cell must dissipate a larger amount of waste heat. Thus increasing the current density can lead to nonuniform temperature distribution in the cell. The variations of maximum temperature in the membrane and the minimum temperatures in the GDLs are shown in

Fig. 2.3. As expected, both the maximum and minimum temperatures in the cell increase as the current density increases. It is also seen that the difference between the two temperatures also increases with increasing current density. It should be noted that the relationship between temperatures and current density is expected to be nonlinear. However, as the total temperature rise is only a few degrees, the nonlinearity is not reflected in the results.

It can also be observed that the difference between the two temperatures is more than 2K beyond a current density of around 6000 A/m^2. Such a temperature difference will produce a difference in the saturation pressure of about 4-5 kPa which may be of significant concern for dry-out or flooding behavior inside the fuel cell.

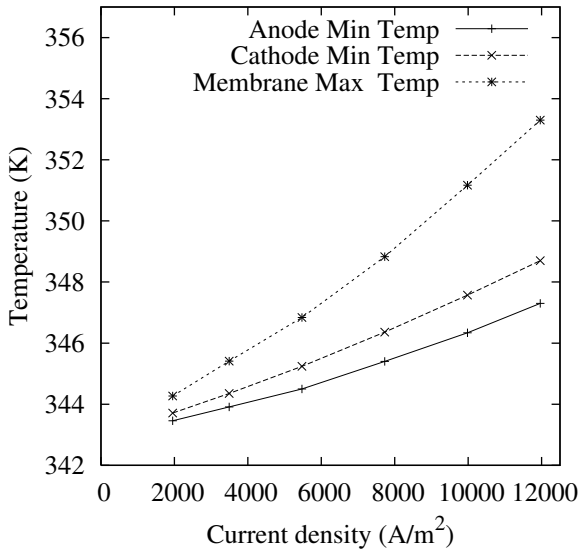

Fig. 2.3 Variation of membrane and GDL temperatures with current density.

2.4.3 Effect of thermal contact conductance

It was shown in Sec. 2.4.1 that the thermal contact conductance at the interface between the current collector and GDL can affect the temperature distribution by an appreciable amount. Figure 2.4 shows the temperature distributions for two values of the contact conductance. All other parameters were kept the same as that for the base case. Also, even though the geometry of Fig. 2.4 is same as that of Fig. 2.2, the entire current collector plate is not shown as the temperature in the current collector plates is practically uniform because of their high thermal conductivity.

It is seen that the temperatures inside the MEA increase with decreasing thermal contact conductance. A larger area or volume of the membrane is now at a high

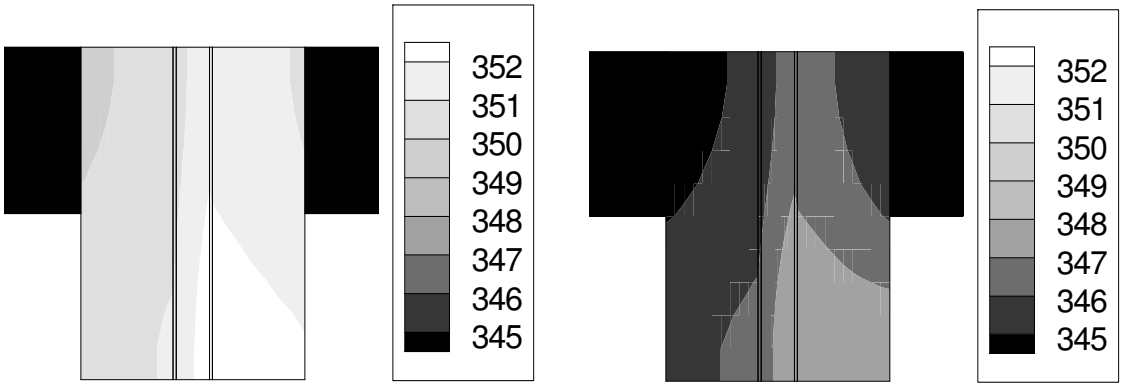

(a) (b)

Fig. 2.4 Temperature distribution for two values of thermal contact conductance: (a) $h_{contact}$ = 500 W/m^2-K and (b) $h_{contact}$ = 10000 W/m^2-K.

temperature. This can lead to a serious deterioration of the membrane properties, including dry-out. However, higher temperatures in the cathode GDL can lead to reduced tendency for condensation, and the temperatures also tend to be more uniform throughout the MEA. Higher temperatures reduce the membrane ionic conductivity by reducing the

water vapor activity and increase the cathode reaction rate. In general however, the current density at given voltage is more severely affected by the change in membrane ionic conductivity than the corresponding increase in cathode reaction rate. Hence, it is desirable to have lower temperatures in the membrane and hence a high value of thermal contact conductance.

A higher value of the contact conductance also results in lower temperatures in the GDLs. This can exacerbate problems related to condensation. Therefore, a technique is needed to reduce the temperatures in the membrane without creating low temperatures in the GDLs.

2.4.4 Effect of anisotropy in thermal conductivity of the gas-diffusion layer

As mentioned previously, the heat generated in the cathode catalyst layer and the membrane must be effectively transferred to the current collector (cooling plate) via the GDLs. The GDLs are constructed from porous, fibrous materials. Their thermal conductivity is expected to be anisotropic, depending on the orientation of the fibers. One possible approach to achieve effective heat transfer is to increase the in-plane thermal conductivity of the GDL. The effect of changing the in-plane thermal conductivity on the overall temperature distribution of the cell is shown Fig. 2.5. The normal thermal conductivity was kept constant at the base-case value and the in-plane conductivity was varied.

It is seen that a low value of the in-plane thermal conductivity results in high temperatures in the membrane and formation of a hot spot. The average temperature in

the GDLs in contact with the current collectors is lower than in the isotropic case. This leads to a higher probability of problems associated with condensation in the GDLs. Such a condition is thus highly undesirable. A higher value of the in-plane thermal conductivity, however, leads to a much more uniform temperature distribution. The maximum temperature is also lower than the situation involving a low in-plane thermal conductivity, as shown in Fig. 2.5. Thus, it would be highly desirable to tailor the GDLs to have a high value of the in-plane thermal conductivity.

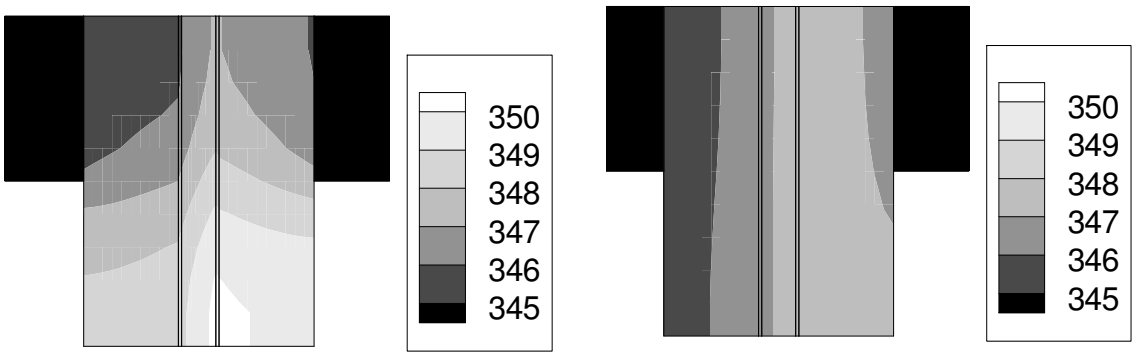

(a) (b)

Fig. 2.5 Effect of anisotropy in thermal conductivity of GDLs on temperature distribution: (a) $k_{yy}/k_{xx} = 0.33$ and (b) $k_{yy}/k_{xx} = 10$.

2.4.5 Effect of anisotropic thermal conductivity of the membrane

Nafion is generated by copolymerization of a perfluorinated vinyl ether comonomer with tetrafluoroethylene (TFE) and made into sheets through an extrusion process. This extrusion process can cause a preferential orientation of fibers in the flow direction [50]. Hence, the thermal conductivity of the membrane can be expected to be higher in the in-plane direction. The effect of anisotropic thermal conductivity of the

membrane on the temperature distribution inside the cell is shown in Fig. 2.6. It appears that the anisotropic membrane thermal conductivity may not have a significant impact on the temperature distribution in the cell unless the thermal conductivity is extremely low or unless the membrane thickness is significantly increased.

2.4.6 Effect of gas-diffusion layer thickness

The thickness of the GDL tends to be different depending on the manufacturer. The effect of changing thickness of the GDLs is shown in Fig. 2.7. The temperature distributions are shown for two extreme values of thicknesses. It can be seen that, as

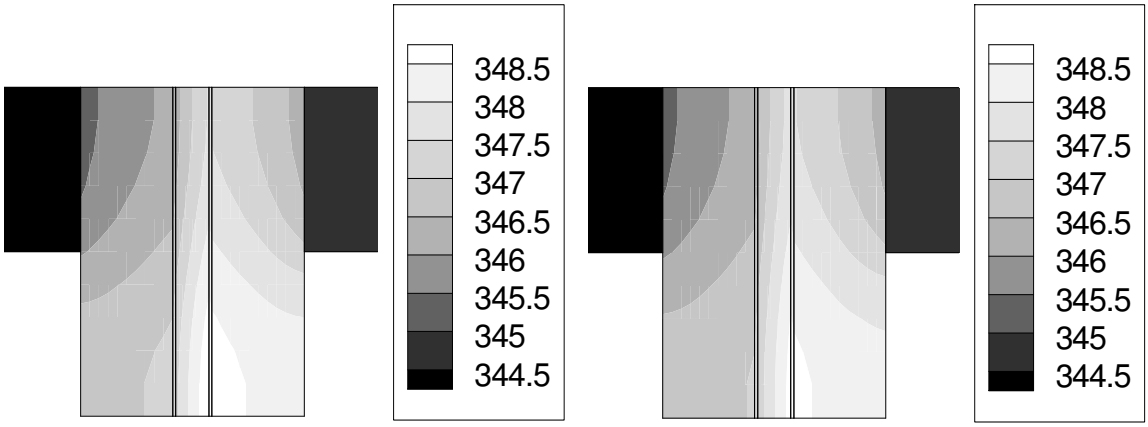

(a) (b)

Fig. 2.6 Effect of anisotropy in thermal conductivity of membrane on temperature: (a) $k_{yy}/k_{xx} = 0.33$ and (b) $k_{yy}/k_{xx} = 10.0$.

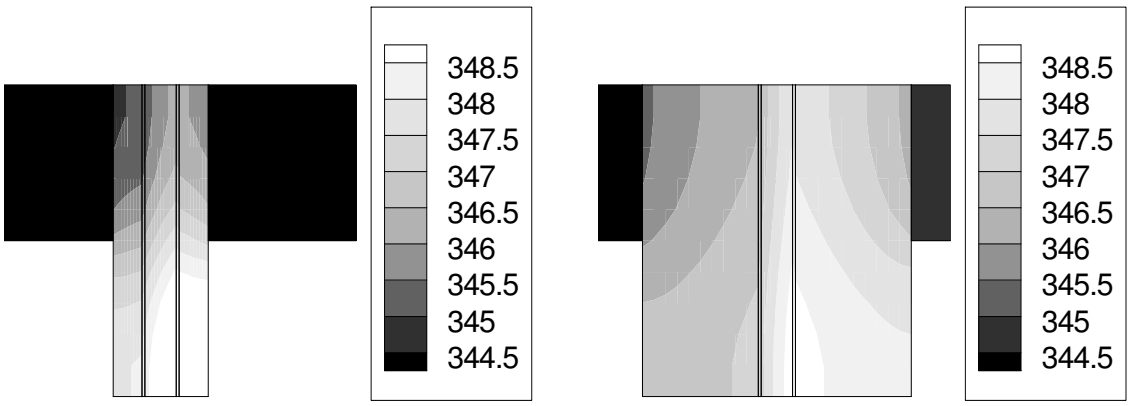

(a) (b)

Fig. 2.7 Effect of GDL thickness on temperature distribution inside the cell: (a) thickness = 100 μm and (b) thickness = 400 μm.

expected, a greater thickness leads to an increase in the area at higher temperatures in the membrane. It can also be noted that in case of a thin GDL, the complete upper half of the cell has lower temperatures than the lower half. A thin GDL, even though desirable from a mass diffusion point of view, can lead to low temperatures and cause condensation problems. The lower temperatures in this region can also cause reduced reaction rates in spite of a possible reduction in the resistance to diffusion of the reactant gases. A thin diffusion layer in fact makes it more difficult for the reactant gases to reach the catalyst area below the current collector since the area for the flow of the reactants is reduced. The resistance to diffusion of reactant gases reduces only in the region of GDL directly exposed to the gas channel. Thus, the reactant concentration is not high for the thin diffusion layer below the current collector and does not compensate for lower temperatures in the region below the current collectors. Hence, in case of thin GDLs, it is especially important to have a high value of the in-plane thermal conductivity.

It can thus be seen that thermal contact conductance at the GDL/current collector interface, in-plane GDL conductivity and the GDL thickness are the most important factors affecting the heat transfer characteristics. These factors are subject to optimization within practical limits to achieve the most uniform temperature distribution inside the cell. The next section analyzes the limits on the optimum heat transfer performance that can be obtained by varying these parameters and the reasons for those limits.

2.4.7 Optimum heat transfer performance and approximate analysis

The variation of maximum cell temperature with the in-plane thermal conductivity for different GDL thicknesses is shown in Fig. 2.8. It can be seen that the

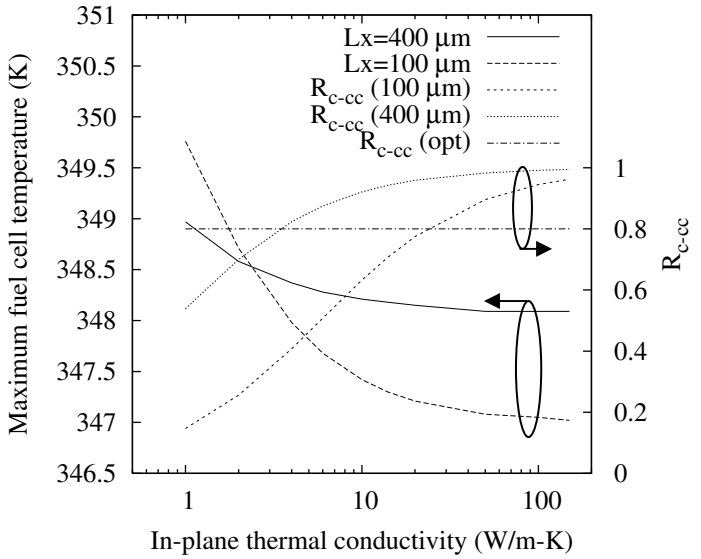

Fig. 2.8 Variation of maximum fuel cell temperature with increasing in-plane thermal conductivity.

maximum temperature for the isotropic case is higher for the thinner GDL. Thus the maximum cell temperature does not reduce with thickness of the GDL as intuitively

expected. It can also be seen that the net decrease in temperature obtained by increasing the in-plane thermal conductivity reduces with increasing thickness of the GDL. Thus there is a greater scope to obtain better heat transfer characteristics by increasing the in-plane thermal conductivity in case of a thin GDL. It is also seen that in both the cases the maximum temperature in the cell initially decreases and then levels off beyond a certain value of the in-plane thermal conductivity. Thus, increasing the in-plane thermal conductivity beyond this point will not lead to any substantial improvements in the heat transfer characteristics. These trends in heat transfer in the cell can be explained using the following approximate analysis.

The schematic for the approximate analysis along with the possible heat flow paths from the high temperature region is shown in the Fig. 2.9. The heat generated in the MEA can either be dissipated to the gas flowing in the channel, or it can be conducted to the current collector, which itself has a high thermal conductivity. The resistance to heat transfer to the gas channel and current collector are, respectively, approximately given by

$$R_{gc} = \frac{L_x}{k_{xx} L_{y1}} + \frac{1}{h_{gas} L_{y1}} \tag{2.17a}$$

$$R_{cc} = \frac{L_{y1}}{k_{yy} L_x} + \frac{L_x}{k_{xx} L_{y2}} + \frac{1}{h_{contact} L_{y2}} \tag{2.17b}$$

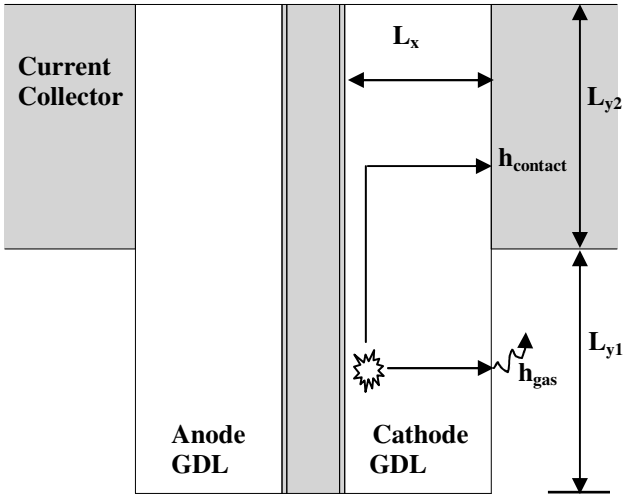

Fig. 2.9 A simplified view of heat transfer in a fuel cell.

The convective resistance to heat flow at the GDL/gas channel boundary is about 2-4 times larger than any other resistance in the cell (for the base-case condition parameters chosen in this analysis). Thus most of the heat flows through the current collector via its interface to the GDL. Thus heat transfer characteristics can be improved by reducing the resistance to heat flow towards the current collector. It can also be noticed from the discussion in the previous section that as the hotspot is formed near the midpoint of the gas channel, the resistance to flow in the in-plane direction is the most critical resistance determining the maximum temperature in the fuel cell. In this context, it is useful to define the following dimensionless parameter using Eq. (2.17b): the ratio of the net normal and interfacial resistance to the total resistance ($R_{c\text{-}cc}$) given by

$$R_{c-cc} = \frac{\dfrac{L_x}{k_{xx} L_{y2}} + \dfrac{1}{h_{contact} L_{y2}}}{\dfrac{L_{y1}}{k_{yy} L_x} + \dfrac{L_x}{k_{xx} L_{y2}} + \dfrac{1}{h_{contact} L_{y2}}} \tag{2.18}$$

The above ratio thus indicates the relative importance of the thermal contact resistance and the normal resistance for the flow of heat towards the current collector. A low value of the above ratio would indicate that the maximum temperature in the cell can be reduced by increasing the in-plane thermal conductivity.

It was shown earlier in this section that a reduction in the GDL thickness results in an increase in the maximum temperature in the cell. It can be seen from Eq. (2.17b) that a reduction in the GDL thickness decreases the normal resistance (second term in Eq. 2.17b) and increases the in-plane resistance (first term in Eq. 2.17b), which is also the larger of the two resistances ($L_{y1} > L_x$ generally). As seen earlier, the in-plane resistance is the most critical resistance determining the maximum temperature in the cell and hence the cell temperature increases. It was also observed that the maximum temperature in the cell levels off beyond a certain value of the in-plane thermal conductivity. This is because the ratio $R_{c\text{-}cc}$ reaches a limiting high value beyond which heat transfer can be improved only by increasing the thermal contact conductance. This also explains the fact that the reduction in maximum temperature for thick GDLs is lower than thin GDLs as the limiting value of $R_{c\text{-}cc}$ is reached earlier in the former case as shown in Fig. 2.8. Thus, in view of the numerical results presented in this chapter, the limiting condition for optimizing the heat transfer characteristics in the fuel cell is given as

$$R_{c\text{-}cc} = 0.8 \tag{2.19}$$

for all practical purposes (see Fig. 2.8). This condition can be used to determine the optimum combination of GDL thickness and in-plane thermal conductivity for minimizing temperature gradients within the cell.

2.5 Conclusions

We present a parametric study on the possible effects of anisotropic thermal conductivity and contact conductance on the temperature distribution inside a fuel cell. The analysis leads to some important insights into the temperature distribution of the cell. Based on the chosen set of operating conditions, the following conclusions can be drawn from the analysis.

1. A low value of thermal contact conductance at the GDL/current collector interface can lead to high temperatures inside the fuel cell. This contact conductance is the single most important factor controlling the temperature distribution.
2. The thermal conductivity of GDLs can have a great impact on the temperature gradients. It is desirable to have a high in-plane thermal conductivity for the GDL from heat transfer point of view. However there exists an optimum value of the in-plane thermal conductivity beyond which no significant improvement in heat transfer characteristics can be obtained simply by increasing the thermal conductivity.
3. Thin GDLs lead to a highly non-uniform distribution of temperature. However, there is a greater scope for reducing the temperature gradients by increasing the in-plane thermal conductivity in case of thin GDLs than the thicker GDLs.
4. However, anisotropic behavior of the thermal conductivity of the proton-exchange membrane does not have a serious impact on the cell operation due to its thinness.

It must be noted that the above results are based on a single-phase model, which neglects the effects of vapor condensation and associated mass transfer limitations. Moreover, the current study concentrates only on the heat transfer aspects of the fuel cell performance. A more detailed analysis using a more comprehensive model is presented in the next chapter.

2.6 References

[1] Springer, T. E., Zawodzinski, T. A., and Gottesfeld, S., 1991, *J. Electrochem. Soc.*, vol. 138, p. 2334.

[2] Bernardi, D. M., and Verbrugge, M. W., 1991, *AIChE J.*, vol. 37, p. 1151.

[3] Bernardi, D. M., and Verbrugge, M. W., 1992, *J. Electrochem. Soc.*, vol. 139, p. 2477.

[4] Fuller, T. F., and Newman, J., 1993, *J. Electrochem. Soc.*, vol. 140, p. 1218.

[5] Nguyen, T. V., and White, R. E., 1993, *J. Electrochem. Soc.*, vol. 140, p. 2178.

[6] Djilali, N., and Lu, D., 2002, *Int. J. Therm. Sci.*, vol. 41, p. 29.

[7] Bevers, D., Wohr, M., Yasuda, K., and Oguro, K., 1997, *J. Appl. Electrochemistry*, vol. 27, p. 1254.

[8] Wohr, M., Bolwin, K., Schnurnberger, W., Fischer, M., Neubrand, W., and Eigenberger, G., 1998, *Int. J. Hydrogen Energy*, vol. 23, p. 213.

[9] Rowe, A., and Li, X., 2001, *J. Power Sources*, vol. 102, p. 82.

[10] Dutta, S., Shimpalee, S., and Van Zee, J. W., 2000, *J. Appl. Electrochemistry*, vol. 30, p. 135.

[11] Um, S., Wang, C. Y., and Chen, K. S., 2000, *J. Electrochem. Soc.*, vol. 147, p. 4485.

[12] Um, S., and Wang, C. Y., 2003, *J. Power Sources*, vol. 125, p. 40.

[13] Berning, T., Lu, D. M., and Djilali, N., 2002, *J. Power Sources*, vol. 106, p. 284.

[14] Zhou, T., and Liu, H., 2001, *Int. J. Trans. Phenomena*, vol. 3, p. 177.

[15] Ju, H., Meng, H., and Wang, C. Y., 2005, *Int. J. Heat Mass Transfer*, vol. 48, p. 1303.

[16] Sivertsen, B. R., and Djilali, N., 2005, *J. Power Sources*, vol. 141, p. 65.

[17] Baschuk, J. J., and Li, X., 2000, *J. Power Sources*, vol. 86, p. 181.

[18] Stockie, J. B., 2002, *Proceedings of IMECE'02, 2002 ASME International Mechanical Engineering Congress and Exposition*, HTD-Vol. 7, p. 393.

[19] Berning, T., and Djilali, N., 2003, *J. Electrochem. Soc.*, vol. 150, p. A1589.

[20] Wang, C. Y., and Cheng, P., 1997, *Adv. Heat Transfer*, vol. 30, p. 93.

[21] Wang, Z. H., Wang, C. Y., and Chen, K. S., 2001, *J. Power Sources*, vol. 94, p. 40.

[22] Wang, C. Y., and Cheng, P., 1996, *Int. J. Heat Mass Transfer*, vol. 39, p. 3607.

[23] Hu, M., Gu, A., Wang, M., Zhu, X., and Yu, L., 2004, *Energy Convers. Manage.*, vol. 45, p. 1861.

[24] Hu, M., Zhu, X., Wang, M., Gu, A., and Yu, L., 2004, *Energy Convers. Manage.*, vol. 45, p. 1883.

[25] Mazumder, S., and Cole, J. V., 2003, *J. Electrochem. Soc.*, vol. 150, p. A1510.

[26] Sun, H., Liu, H., and Guo, L., 2005, *J. Power Sources*, vol. 143, p. 125.

[27] Birgersson, E., Noponen, M., and Vynnycky, M., 2005, *J. Electrochem. Soc.*, vol. 152, p. A1021.

[28] Shimpalee, S., Greenway, S., Spuckler, D., and Van Zee, J. W., 2004, *J. Power Sources*, vol. 135, p. 79.

[29] Baschuk, J. J., and Li, X., 2004, *J. Power Sources*, vol. 142, p. 134.

[30] Nam, J. H., and Kaviany, M., 2003, *Int. J. Heat Mass Transfer*, vol. 46, p. 4595.

[31] Pasaogullari, U., and Wang, C. Y., 2004, *Electrochimica Acta*, vol. 49, p. 4359.

[32] Pasaogullari, U., and Wang, C. Y., 2005, *J. Electrochem. Soc.*, vol. 152, p. A380.

[33] Yuan, J., Rokni, M., and Sundén, B., 2003, *Num. Heat Transfer, Part A*, vol. 44, p. 255.

[34] Musser, J., and Wang, C. Y., 2000, *Proceedings of NHTC'00, 34th National Heat Transfer Conference*, NHTC-Vol. 1, p. 291.

[35] Mawardi, A., Yang, F. and Pitchumani, R., 2005, *J. Fuel Cell Sci. Tech.*, vol. 2, p.121.

[36] Kurabayashi, K., 2001, *Int. J. Thermophysics*, vol. 12, p. 277.

[37] Hansen, D., and Bernier, G. A., 1972, *Poly. Eng. Sci.*, vol. 12, p. 204.

[38] Morelli, D. T., Heremans, J., Sakomoto, M., and Uher, C., 1986, *Phys. Rev. Letters*, vol. 57, p. 869.

[39] Kurabayashi, K., Asheghi, M., Touzelbaev, M., and Goodson, K. E., 1999, *IEEE J. Microelectro. Sys.*, vol. 8, p. 180.

[40] Newman, J. S., 1973, *Electrochemical Systems*, Prentice Hall, Englewood Cliffs, N.J.

[41] Shah, R. K., London, A. L., 1978, *Laminar Flow Forced Convection in Ducts*, Academic Press, New York.

[42] Parthasarathy, A., Srinivasan, S., and Appleby, J. A., 1992, *J. Electrochem. Soc.*, vol. 139, p. 2530.

[43] Mirmira, S. R., Marotta, E. E., and Fletcher, L. S., 1998, *J. Thermophys. Heat Transfer*, vol. 12, p. 454.

[44] Marotta, E. E., and Fletcher, L. S., 1996, *J. Thermophys. Heat Transfer*, vol. 10, p. 334.

[45] Fuller, J. J., and Marotta, E. E., 2001, *J. Thermophys. Heat Transfer*, vol. 15, p. 228.

[46] Hollinger, A., 2006, *Contact Resistance Measurements of Gas-diffusion layers and Membrane for Fuel Cell Applications*, Senior Honors Thesis, Department of Engineering Science and Mechanics, The Pennsylvania State University, University Park, PA.

[47] Mishra, V., Yang, F., and Pitchumani, R., 2004, *J. Fuel Cell Sci. Technol*., vol. 1, p. 2.

[48] Wang, L., Husar, A., Zhou, T., and Liu, H., 2003, *Int. J. Hydrogen Energy*, vol. 28, p. 1263.

[49] Patankar, S. V., 1980, *Numerical Heat Transfer and Fluid Flow*, Hemisphere, Washington, D.C.

[50] Mauritz, K. A. and Moore, R. B., 2004, *Chem. Rev.*, vol. 104, p. 4535.

Chapter 3

Two-phase effects

3.1 Introduction

Liquid water is produced in the cathode catalyst layer due to electrochemical reactions. Excessive amount of liquid water in the cathode GDL reduces the flow of reactants to the catalyst layer by clogging the GDL pores. It also reduces the reaction rate by covering the reaction sites [1]. The amount of liquid water accumulated in the cathode GDL depends on many factors, including the temperature distribution inside the cell as it controls the phase change of water. Over the past few years many different models have been developed to analyze the water and heat management problems in a fuel cell. The earliest models [2-6] did not include an explicit two-phase model to account for the liquid water transport in the catalyst layers and GDLs. Thus, these single-phase models were unable to accurately predict the polarization behavior at high current densities where the effects of liquid water accumulation are most severe [7]. Hence, different two-phase models were developed [7-20] to account for the effect of liquid water transport. The two-phase models were based on the unsaturated flow theory [21] or the multiphase mixture model [22]. Meng [23] and Weber and Newman [24, 25] further improved models for water transport in the ionic membrane. The effects of various flow and transport properties on the polarization behavior were analyzed using these single-phase and two-phase models.

The effect of the thermal conductivity of the GDLs on polarization behavior was analyzed by Ju et al. [26] using a single-phase model. The authors also assumed the GDL thermal conductivity to be isotropic. The GDLs are commonly constructed of carbon fibers either in woven or paper form. Electron micrographs for different GDLs [27] suggest that the carbon fibers are preferentially oriented in the in-plane direction. The thermal conductivity measurements for polymers with preferential fiber orientation [28-31] and also for certain GDLs [32, 33] suggest that the thermal conductivity of the GDLs is highly anisotropic. The effect of anisotropic thermal conductivity on multicomponent transport in a fuel cell cathode was considered by Pasaogullari et al. [34] using the multiphase mixture model [22] and by Pharoah et al. [35] using a single-phase model. In this chapter, we extend the model developed previously [36] to present an analysis of the effect of both the magnitude and anisotropy of the GDL thermal conductivity on polarization characteristics at low and high humidity operating conditions using a two-dimensional two-phase model. We also analyze the effect of current collector rib width on polarization behavior. We use the classical two-fluid model proposed by Ishii [37], Drew and Passman [38] and Hassanizadeh and Gray [39, 40] in our work and also account for the effect of electrical and thermal contact resistance at the GDL/bipolar plate interface. In the next section we describe in detail the mathematical model used for our work.

3.2 Model formulation

The model presented here (Table 3.1) accounts for flow of reactants, products and ionic species, as well as the generation and transport of heat. The two-dimensional computational domain used in chapter is shown in Fig. 1.1. The assumptions and simplifications used in our model are described next.

Table 3.1 Model equations and source terms

Equation	Ref.
Electrochemical reactions:	
$-\nabla\cdot(\kappa\nabla\phi_m)=FS^{H^+}$	
$FS^{H^+}=j_c=\alpha_g i_{oc}^{ref}\left[\exp\left\{\frac{\alpha_a F}{RT}(\phi_s-\phi_m)\right\}-\exp\left\{-\frac{\alpha_c F}{RT}(\phi_s-\phi_m)\right\}\right]\left(\frac{C_g^{O_2}}{C_{ref}^{O_2}}\right)+\alpha_l i_{oc}^{ref}\left[\exp\left\{\frac{\alpha_a F}{RT}(\phi_s-\phi_m)\right\}-\exp\left\{-\frac{\alpha_c F}{RT}(\phi_s-\phi_m)\right\}\right]\left(\frac{C_l^{O_2}}{C_{ref}^{O_2}}\right)$ at cathode	
$FS^{H^+}=j_a=\alpha_g i_{oa}^{ref}\left[\exp\left\{\frac{\alpha_a F}{RT}(\phi_s-\phi_m)\right\}-\exp\left\{-\frac{\alpha_c F}{RT}(\phi_s-\phi_m)\right\}\right]\left(\frac{C_g^{H_2}}{C_{ref.}^{H_2}}\right)^{\frac{1}{2}}+\alpha_l i_{oa}^{ref}\left[\exp\left\{\frac{\alpha_a F}{RT}(\phi_s-\phi_m)\right\}-\exp\left\{-\frac{\alpha_c F}{RT}(\phi_s-\phi_m)\right\}\right]\left(\frac{C_l^{H_2}}{C_{ref.}^{H_2}}\right)^{\frac{1}{2}}$ at anode	
Gas/Liquid phase species transport:	
For $i = O_2, H_2, N_2$	
$\frac{\partial\varepsilon\alpha_{g/l}C_{g/l}^i}{\partial t}+\nabla\cdot(\varepsilon\alpha_{g/l}C_{g/l}^i\mathbf{v}_{g/l})=\nabla\cdot(\varepsilon\alpha_{g/l}D_{g/l}^i\nabla C_{g/l}^i)\mp\gamma_{\mathrm{lg}}^i\left(\frac{RT}{K_H^i}C_g^i-C_l^i\right)A_{\mathrm{lg}}+S_{g/l}^i$	[39]
In catalyst layers	[40]

$$S_{g/l}^{O_2} = \frac{1}{4F}\alpha_{g/l} i_{oc}^{ref}\left[\exp\left\{\frac{\alpha_a F}{RT}(\phi_s - \phi_m)\right\} - \exp\left\{-\frac{\alpha_c F}{RT}(\phi_s - \phi_m)\right\}\right]\left(\frac{C_{g/l}^{O_2}}{C_{ref}^{O_2}}\right)$$

$$S_{g/l}^{H_2} = -\frac{1}{2F}\alpha_{g/l} i_{oa}^{ref}\left[\exp\left\{\frac{\alpha_a F}{RT}(\phi_s - \phi_m)\right\} - \exp\left\{-\frac{\alpha_c F}{RT}(\phi_s - \phi_m)\right\}\right]\left(\frac{C_{g/l}^{H_2}}{C_{ref.}^{H_2}}\right)^{\frac{1}{2}}$$

and $S_{g/l}^{i} = 0$ everywhere else. Nitrogen does not take part in chemical reactions.

Component balance for water:

In catalyst layers and GDLs

$$\frac{\partial \varepsilon \alpha_{g/l} C_{g/l}^{H_2O}}{\partial t} + \nabla \cdot (\varepsilon \alpha_{g/l} C_{g/l}^{H_2O} \mathbf{v}_{g/l}) = \nabla \cdot (\varepsilon \alpha_{g/l} D_{g/l}^{H_2O} \nabla C_{g/l}^{H_2O}) \mp \gamma_{\lg}^{H_2O}\left(C_g^{H_2O} - \frac{P_{sat,H_2O}}{RT}\right)A_{\lg} + S_{g/l}^{H_2O} \quad [39]$$

In membrane

$$\frac{\partial \varepsilon \alpha_g C_g^{H_2O}}{\partial t} = \nabla \cdot (\varepsilon \alpha_g D_g^{H_2O} \nabla C_g^{H_2O}) + S_g^{H_2O} \quad [40]$$

$S_g^{H_2O} = -\nabla \cdot \left(\frac{n_{oe}}{F}\mathbf{i}\right)$ in membrane and catalyst layers

$S_l^{H_2O} = -\frac{j_c}{2F}$ in cathode catalyst layer

Two phase momentum balance:

$$\frac{\partial \varepsilon \alpha_{g/l} \rho_{g/l} \mathbf{v}_{g/l}}{\partial t} + \nabla \cdot \varepsilon \alpha_{g/l} \rho_{g/l} \mathbf{v}_{g/l} \mathbf{v}_{g/l} = -\nabla \varepsilon \alpha_{g/l} p_{g/l} + \nabla \cdot \varepsilon \alpha_{g/l} \tau_{g/l} - \frac{\mathbf{v}_{g/l} \mu_{g/l}}{K_p K_{g/lr}} \quad [39]$$

and $p_l = p_g - p_c$ [40]

Heat balance equation:

$$\frac{\partial}{\partial t}\left(\rho_{eq} c_{eq} T\right) + \nabla \cdot \left(\varepsilon \alpha_l \rho_l \mathbf{v}_l c_l T\right) + \nabla \cdot \left(\varepsilon \alpha_g \rho_g \mathbf{v}_g c_{pg} T\right)$$
$$= \nabla \cdot \left(\mathbf{k}_{eq} \cdot \nabla T\right) + \gamma_{\lg}^{H_2O}\left(C_g^{H_2O} - \frac{P_{sat,H_2O}}{RT}\right)A_{\lg} M^{H_2O} L_w + \dot{q}'''$$

$$\rho_{eq} c_{eq} = (1-\varepsilon)\rho_{por} c_{por} + \varepsilon \alpha_l \rho_l c_l + \varepsilon \alpha_g \rho_g c_{pg}$$

$$\mathbf{k}_{eq} = (1-\varepsilon)\mathbf{k}_{por} + \varepsilon\alpha_l \mathbf{k}_l + \varepsilon\alpha_g \mathbf{k}_g$$

where

$\dot{q}''' = \mid j_a(\phi_s - \phi_m) \mid + \dfrac{i^2}{\kappa}$ in anode catalyst layer

$\dot{q}''' = \dfrac{i^2}{\kappa}$ in membrane

$\dot{q}''' = \mid j_c(\phi_s - \phi_m) \mid + \dfrac{i^2}{\kappa} + \mid T\Delta S \dfrac{j_a}{2F} \mid$ in cathode catalyst layer

$\dot{q}''' = i_{tot}^2 \sigma$ in GDLs

$\dot{q}''' = \dfrac{(i_{tot} A)^2 R_{ccontact}}{\Delta V_{net}}$ for a computational cell adjacent to GDL/bipolar plate interface

Also see Table 3.2 for a simplified expression for $\mathbf{k}_{eq}$.

3.2.1 Flow model

We use a two-phase model to analyze transport of species in the catalyst layers and GDLs. As stated in section 1, the two-phase transport of different species is modeled using the classical two-fluid model proposed by Ishii [37], Drew and Passman [38] and Hassanizadeh and Gray [39, 40]. The porous drag is modeled using a source term based on the Darcy law. The effects of phase change and species dissolution are modeled using rate expressions which account for the effect of gas-liquid interfacial area density.

We use a single-phase model for transport inside the membrane, this means that the liquid water produced at cathode is not allowed to enter the membrane and consider

only the concentration-driven diffusion of water vapor through the membrane. We also do not consider phase change of water inside the membrane. The assumption of single-phase transport inside the ionic membrane seems reasonable for two reasons: the hydraulic permeability of the membrane is a few orders of magnitude lower than the hydraulic permeability of the GDL and the membrane is known to be at least slightly hydrophobic with pore radii much smaller than the GDL [24, 25]. The overall effect of using a single-phase model in the membrane is to slightly overestimate the effects of liquid water accumulation in catalyst layers and GDLs on polarization behavior.

3.2.2 Heat transport model

We also assume that the gas and liquid phases as well as the porous matrix are in local thermal equilibrium. Hence we use a single equation derived by summation of the respective phase heat transport equations to estimate the temperature distribution. The heat generation is modeled using appropriate source terms in different regions of the fuel cell. The model accounts for heat generation due to

1. activation polarization in catalyst layers,
2. ohmic polarization in catalyst layers and the ionic membrane,
3. reversible heat loss,
4. phase change and
5. flow of electric current in the GDLs and at the GDL/bipolar plate interface.

Also, the entire reversible heat loss is assumed to occur in the cathode catalyst layer.

3.2.3 Electrochemistry

We solve for transport of protons in the catalyst layers and membrane. The solid-phase potential in the catalyst layers is assigned according to the boundary conditions. The effect of electrical contact resistance is also taken into account in the boundary conditions. The electrochemical reactions are modeled by the Butler-Volmer reaction rate expressions [41] which are modified to include the effect of liquid accumulation on the reaction rates by assuming proportionality to the phase volume fractions.

3.2.4 Channel flow model

We solve for pressures and component balances in the channels to determine the pressures and concentrations of different species at different distances from the inlet. The pressures and concentrations so determined are then used as boundary conditions for the two-dimensional model used in our work. This allows us to simulate the polarization behavior at different distances form the inlet.

The pressure variation is calculated using the Darcy friction factor law [42] to account for the effect of wall friction. The reactant concentrations are calculated using simple mass balances accounting for the production/consumption of reactants and products [43]. The water produced at the cathode is assumed to mix with the cathode gas stream in the form of water vapor, and phase change of water vapor in the gas channels is neglected. The temperature change of the reactant gases is also neglected. In spite of these simplifications, the above method of calculating the parameters takes into account

the effect of reactant flow rates, channel length and active area, which otherwise cannot be accounted for in a two-dimensional model. It is noticed that the parameter values calculated above depend on the current density, which is obtained from the solution of the electrochemistry model. Hence the pressure and concentration boundary conditions are also updated during each iteration of the numerical scheme.

3.3 Constitutive relations

In order to complete the description of the model presented in the previous section, constitutive relations for various properties are required. The constitutive relations used in this work are given in Table 3.2. We developed a correlation for the interfacial area density using the existing pore-scale modeling and experimental data [44-46] for different porous media. The correlation is plotted in Fig. 3.1 along with the experimental and modeling data, and it shows an intermediate shape between the model results. We also correlated the available experimental data [47] for diffusivity of water vapor through the ionic membrane. We use the correlation developed by Gostick et al. [48] for capillary pressure in a GDL. The E-Tek carbon cloth used by Gostick and coworkers for their measurements was almost completely hydrophilic, whereas experiments show that the carbon cloth used in the E-Tek electrode (E-Tek electrode has been used in the experimental study used to validate the model) is hydrophobic [49]. Therefore we correct the capillary pressure obtained by their correlation for contact angle. We also express the equivalent thermal conductivity of the GDL (see Table 1) in terms of the thermal conductivity of a dry GDL to facilitate the use of existing

experimental data [50]. We use published correlations for membrane water content at 80°C [51], ionic conductivity [25] and temperature dependence of cathode reaction rate [52].

Table 3.2 Constitutive relations.

Expression	Ref.
Capillary pressure: $\alpha_{wp} = \left(1+\left(\frac{J}{J_c}\right)^n\right)^{-m}$ where $J = \frac{p_{c,Air-water}}{\sigma}\left(\frac{K_p}{\varepsilon}\right)^{\frac{1}{2}}$ and $J_c = 0.6982, n = 3.465, m = 0.7114$ $p_c = p_{c,Air-water}\cos\theta$	[48]
Corrections in property values: $D_g^i = D_{g,o}^i \varepsilon^{1.5}\alpha_g^{3.0}$; $K_{gr} = \alpha_g^{3.0}$, $K_{lr} = \alpha_l^{3.0}$	
Interfacial area density $A_{lg} = 3.14 A_{lgmax}\alpha_l^{0.6}\alpha_g^{1.2}$	See Fig. 3.1
Membrane water content at 80°C $\lambda = 0.300 + 10.8a - 16.0a^2 + 14.1a^3$	[51]
Ionic conductivity $\kappa = 0.5(f-0.06)^{1.5}\exp\left[\frac{15000}{R}\left(\frac{1}{310.0}-\frac{1}{T}\right)\right]$ where $f = \frac{\lambda V_o}{V_m + \lambda V_0}$ and $V_m = \frac{EW}{\rho_m}$	[25]
Vapor diffusivity in the membrane: $D_{g,mem}^{H_2O} = 3.18633\times10^{-10}\,a - 5.23356\times10^{-11}$	

Temperature dependence of exchange current density:

$$i_{oc}^{ref}(T) = i_{oc,o}^{ref}(353K)\exp\left[-\frac{\Delta E}{R}\left(\frac{1}{T}-\frac{1}{353.15}\right)\right] \quad [52]$$

Equivalent thermal conductivity:

The expression for $\mathbf{k}_{eq}$ given in Table 1 can be simplified as,

$$\mathbf{k}_{eq} = \mathbf{k}_{dry} + \varepsilon\alpha_l\left(\mathbf{k}_l - \mathbf{k}_g\right) \qquad \text{where} \qquad \mathbf{k}_{dry} = \begin{bmatrix} k_{xx} & 0 \\ 0 & k_{yy} \end{bmatrix} \quad [50]$$

and k_{xx} and k_{yy} are experimentally measured through-plane and in-plane thermal conductivities. The liquid and gas thermal conductivities are isotropic.

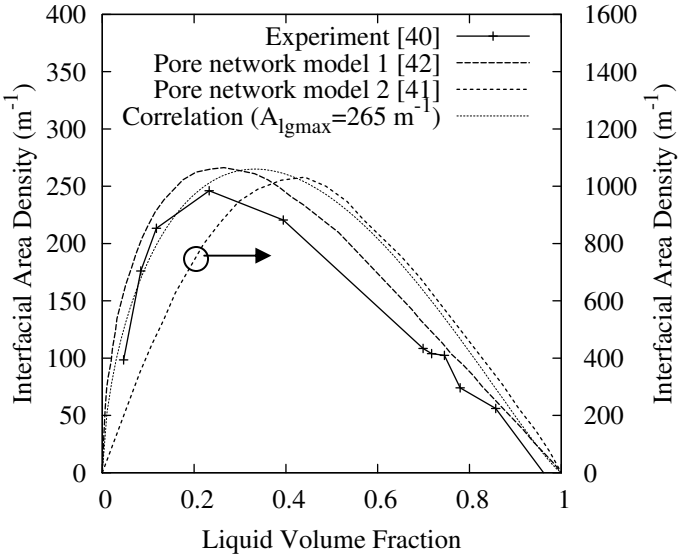

Fig. 3.1 Variation of interfacial area with liquid volume fraction in a porous medium.

3.4 Boundary conditions

The boundary conditions required at various interfaces are now described in detail.

3.4.1 Flow and concentration boundary conditions

The channel pressures as well as the concentrations of reactants and products on the anode and cathode sides are specified as boundary conditions at the GDL/gas channel interfaces. Pressures and concentrations at different distances from the inlet are calculated using the channel flow model described previously. As we use a single-phase model in the ionic membrane, the liquid velocity at the catalyst layer/membrane interface is set to zero.

3.4.2 Electrochemistry

In the current model the electrochemical equations are solved over the MEA. At the GDL/anode interface, they are

$$\phi_s = U_0 - V_{cell} - i_{tot} AR_{acontact} - i_{tot} AR_{gdl} \tag{3.1a}$$

$$\nabla \phi_m = 0 \tag{3.1b}$$

At the GDL/cathode interface, they are

$$\phi_s = i_{tot} AR_{ccontact} + i_{tot} AR_{gdl} \tag{3.2a}$$

$$\nabla \phi_m = 0 \tag{3.2b}$$

Again the analysis presented above is simplified and more complicated issues involving the anisotropic electrical conductivity of the GDLs [32, 33] have not been

addressed. It should also be noted that the above boundary conditions are dependent on the current density. They are also updated during each iteration of the numerical scheme, as in case of the flow boundary conditions. The corresponding heat generation terms due to contact and GDL electrical resistance are also added to the heat equation in the GDLs.

3.4.3 Heat transfer

The heat transfer boundary conditions are same as those used for the single-phase model. They are repeated here for completeness. The heat transfer at the GDL/gas channel interface, current collector/gas channel interface and the current collector/coolant channel interface occurs due to convection. Characteristic *Re* numbers for flow in the gas and coolant channels are low and in the laminar range. Further, the hydrodynamic and thermal entry lengths are relatively short compared to channel lengths. Hence, the convective heat transfer coefficients for the gas and coolant channels are calculated using the following relation applicable for laminar fully developed flows in square channels [53].

$$Nu = \frac{h d_{hyd}}{k_f} = 2.98 \tag{3.3a}$$

where $$d_{hyd} = \frac{4A_{cross}}{P} \tag{3.3b}$$

Additionally, the channel boundaries are at nearly a uniform temperature. The effect of a variable temperature along the GDL boundary on the overall heat transfer coefficient is

neglected. The gas and coolant temperatures were assumed to be at 353K (cell operating temperature).

Also, as the two-dimensional domain used in our work is a symmetrical section, all other boundaries are assumed to obey symmetry boundary conditions.

3.5 Numerical scheme

The set of two-dimensional conservation equations for species, electrochemistry, fluid flow and heat conduction was solved iteratively over the computational domain shown by dotted lines in Fig. 1.1. The values of various parameters used for the model are given in Table 3.3. The heat conduction equation was solved until the relative error in the overall heat balance was $<10^{-3}$, and the flow equations were solved using the SIMPLER scheme [54] (also see appendix) until the relative error mass balance was $<10^{-10}$. The iterations continued until convergence criteria for all the equations were simultaneously met. The solution was obtained for successively refined grids and a Cartesian grid of size 31×10 provided a grid independent solution. The polarization curve was obtained using the model, and the cathode reference exchange current density was used as a fitting parameter [41] along with the catalyst layer porosity. Since the porosity of the E-Tek electrode catalyst layer used in the experiment [55] used for validation is not known, the electrode porosity was used as a fitting parameter for the model. Mench et al. [55] humidify the anode stream to a temperature above the fuel cell operating temperature. Since the fuel cell is maintained at a lower temperature than the anode humidification temperature, the excess water vapor in the anode stream will most

probably condense near the inlet. It is not possible to predict using our model if the water vapor condenses and is carried forward in the form of droplets in the gas stream or if the water vapor condenses at the anode GDL/gas channel interface and then penetrates the anode GDL. Hence for the purposes of this model we assume the anode to be fully humidified at the fuel cell temperature and that none of the condensed water penetrates the anode GDL.

Table 3.3. Model parameters and properties.

Quantity	Value
Gas channel length	1.577 m [55]
Gas channel width	2.16 E-3 m [55]
Current collector width	0.89 E-3 m [55]
Active area	50 E-4 m^2 [55]
Membrane	Nafion® 112 [55]
Gas-diffusion layer thickness	350 E-6 m [48]
Catalyst layer thickness	10.0 E-6 m
Height of the symmetrical section	1.525 E-3 m
Anode humidification temperature	353K [55]
Cathode humidification temperature	353K [55]
Anode inlet stoichiometry	1.875 E4 A m^{-2} equiv [55]
Cathode inlet stoichiometry	1.125 E4 A m^{-2} equiv [55]
Coolant water temperature	353K (assumed)
Cathode inlet pressure	1.5 atm [55]
Anode inlet pressure	1.5 atm [55]

Gas-diffusion layer electrical resistivity	80.0 E-5 ohm-m [32]
Through-plane thermal conductivity of gas-diffusion layers k_{xx}	0.22 W/m-K [50]
Ratio of thermal conductivities k_{yy}/k_{xx}	20:1 (assumed based on [32])
Thermal conductivity of the membrane	0.16 W $m^{-1}K^{-1}$ [50]
Thermal conductivity of the catalyst layer	0.27 W $m^{-1}K^{-1}$ [50]
Thermal conductivity of current collector (steel)	16.0 W $m^{-1}K^{-1}$
GDL/Bipolar plate thermal contact conductance	10000 W $m^{-2}K^{-1}$ (assumed based on [56])
GDL/Bipolar plate electrical contact resistance	41.7 mΩ cm^2 [55]
Gas-diffusion layer porosity	0.74 [49]
Maximum interfacial area density	500 m^{-1}
Catalyst layer porosity	0.15 (fitted)
Hydraulic permeability of GDL	6.3 E-12 m^2 [48]
Hydraulic permeability of membrane	1.0 E-18 m^2 [25]
Hydraulic permeability of catalyst layer	1.0 E-13 m^2 (assumed based on [48])
Contact angle in GDL and catalyst layer	120°
Hydrogen diffusivity	0.915 E-4 m^2 s^{-1} [57]
Oxygen diffusivity	3.0 E-5 m^2 s^{-1} [57]
Water vapor diffusivity	3.0 E-5 m^2 s^{-1} [57]
Electro-osmotic drag coefficient	1.0 [58]
Transfer coefficient at anode $\alpha_a = \alpha_c$	1.0 [20]
Anode reference exchange current density	1.5 E9 A m^{-3} (assumed)

Transfer coefficient at cathode $\alpha_a = \alpha_c$	1.0 $V_{cell} < 0.5$V [52] 0.5 $V_{cell} > 0.5$V
Cathode reference exchange current density	1.1 E2 A m^{-3} $V_{cell} < 0.5$V 3.0 E5 A m^{-3} $V_{cell} > 0.5$V (fitted)
Entropy change ΔS for $H_2 + \frac{1}{2}O_2 \rightarrow H_2O_{(liq.)}$	-162.4 J mol^{-1} K^{-1}

The experimental polarization curves at different distances from the inlet [55] along with the model predictions are shown in Fig. 3.2. It can be seen that even with a two-dimensional model the polarization behavior at different distances from the inlet can be predicted with a good degree of accuracy.

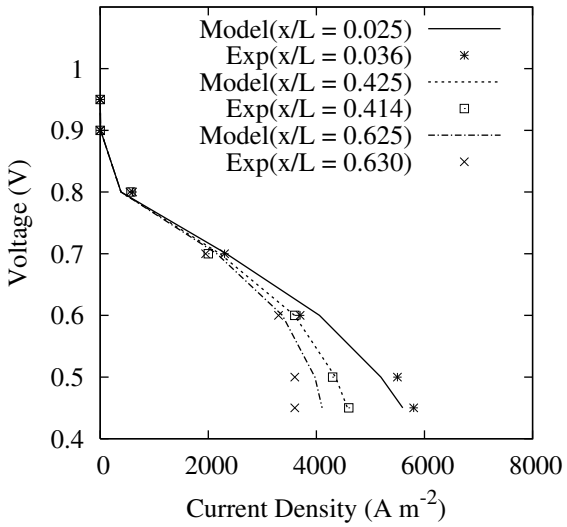

Fig. 3.2 Comparison of experimental [55] and model polarization results.

3.6 Discussion of results

We study the effects of the anisotropic thermal conductivity of the GDLs, as well as the width of the GDLs and current collector ribs on the polarization behavior at different operating conditions. Figure 3.2 shows that the effect of liquid accumulation in the cathode GDL and catalyst layer is more significant at lower voltages. In general, the operating voltage depends on the type of application for which the fuel cell is used. Higher voltages generate lower current densities at higher efficiencies, whereas lower voltages generate higher current densities but at lower efficiencies. We analyze results at three different voltages (0.65V, 0.6V, 0.55V) at which the current densities range from about 50% to 80% of the maximum current density in Fig. 3.2. Also, the inlet flows are generally humidified to maintain the ionic conductivity of the ionic membrane. Therefore, we also investigate the polarization behavior at different cathode inlet humidities. Also, for Figs. 3.3-3.9, values of the parameters kept constant are given in Table 3.3.

3.6.1 Fully humidified cathode inlet

Figures 3.3 and 3.4 show the variations of current density, maximum fuel cell temperature, membrane ionic conductivity and cathode catalyst layer liquid volume fraction near the inlet for different values of in-plane and through-plane thermal conductivities of the GDL. Lower through-plane thermal conductivity leads to higher temperatures. Higher temperatures allow more liquid water to evaporate which reduces

the amount of liquid water accumulated in the cathode catalyst layer. Higher temperatures, however, also reduce the water vapor activity and hence adversely affect the membrane ionic conductivity. Thus increasing the through-plane thermal conductivity of the GDL leads to two competing effects: an increase in the amount of liquid water at the cathode catalyst layer tends to reduce the current density, whereas a higher ionic conductivity of the membrane tends to increase the current density. Since the relative magnitudes of these two competing effects depend on the through-plane thermal conductivity of the GDL, the variation of current density with through-plane thermal conductivity can be expected to show a maximum at a particular value of the through-

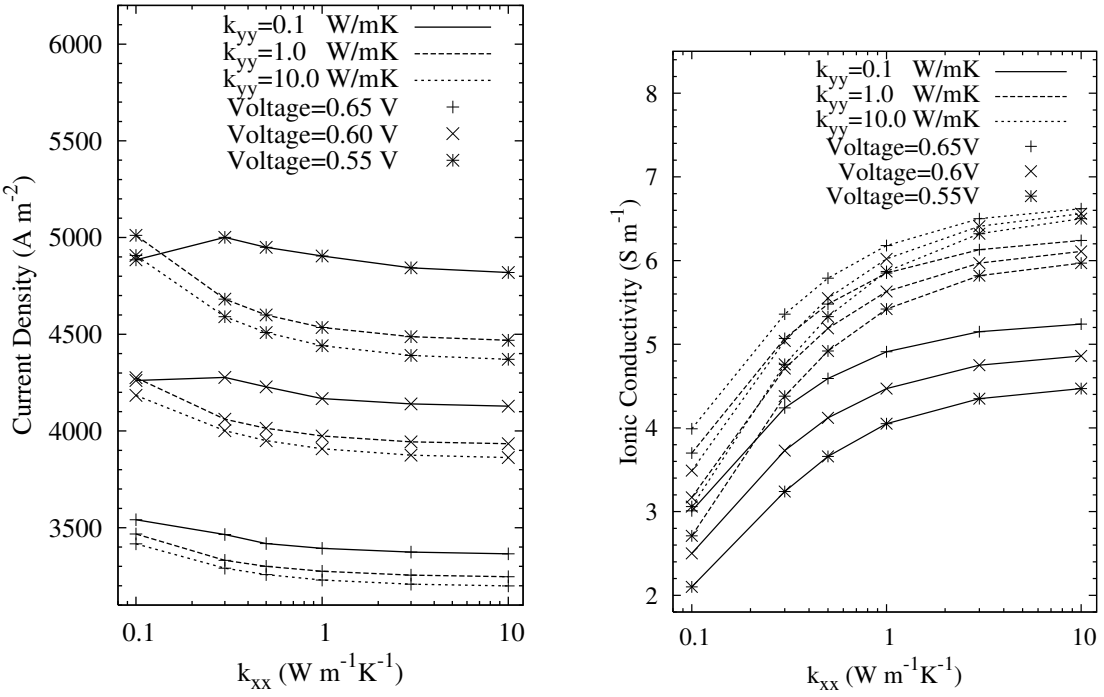

Fig. 3.3 Variation of (a) current density and (b) ionic conductivity with thermal conductivity of the GDL near the inlet for fully humidified cathode inlet flow.

plane thermal conductivity. The variation of current density with increasing through-plane thermal conductivity (see Fig. 3.3a) shows a maximum for low in-plane thermal conductivities at lower voltages. At higher in-plane thermal conductivities, however, the current density decreases with increasing through-plane thermal conductivity for all the

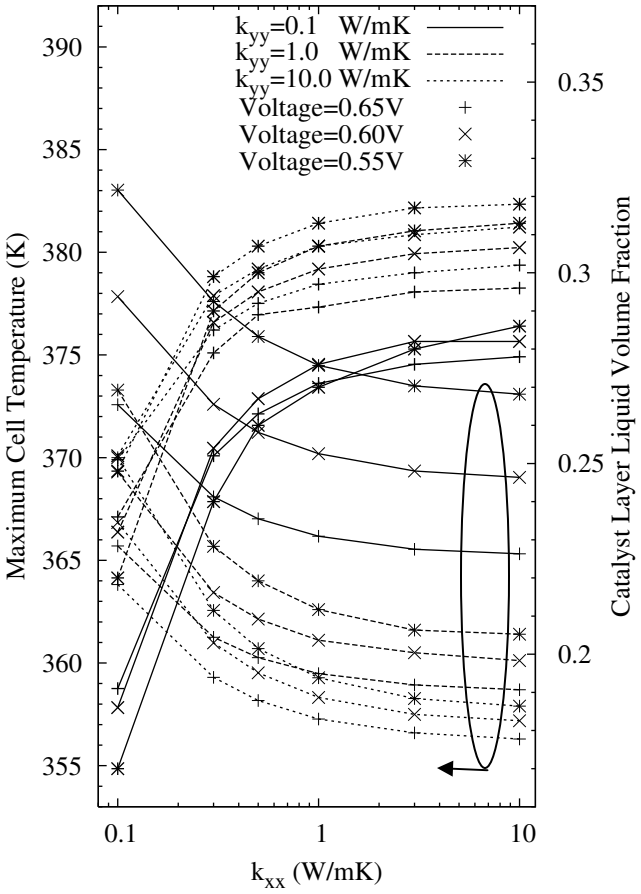

Fig. 3.4 Variation of maximum fuel cell temperature and catalyst layer liquid volume fraction with thermal conductivity of the GDL near the inlet for fully humidified cathode inlet flow.

voltages. Thus, at higher in-plane thermal conductivities, the adverse effect of higher liquid accumulation in the catalyst layer dominates and the current density decreases with

increasing through-plane thermal conductivity. At low in-plane thermal conductivities and lower voltages the temperatures are higher and the membrane ionic conductivities are lower. Hence the variation of current density with increasing through-plane thermal conductivity shows a maximum at lower voltages and lower in-plane thermal conductivities. Lower voltages generate higher current densities which lead to the production of more liquid water and also higher temperatures due to higher heat generation. Hence it is important to determine if the higher temperatures produced at lower voltages are able to evaporate the higher amount of liquid water produced at lower voltages. Figure 3.4 shows that, at lower through-plane thermal conductivities the predicted maximum temperatures are higher for lower voltages. Because of these high temperatures, the liquid water is able to evaporate and liquid accumulation in the cathode catalyst layer is less for lower voltages than that for higher voltages. However, as the through-plane thermal conductivity increases, the temperatures are lowered and the liquid accumulation in the cathode catalyst layer at lower voltages increases to a value above that for higher voltages. Even though higher temperatures reduce the liquid accumulation in the catalyst layer and GDL, such high temperatures also tend to adversely affect the long-term durability of the ionic membrane [59]. Hence it is desirable to achieve higher current densities without creating excessively high temperatures.

The effects of increasing in-plane thermal conductivity on current density, maximum fuel cell temperature, membrane ionic conductivity and cathode catalyst layer liquid volume fraction are also shown in Figs. 3.3 and 3.4. Higher in-plane thermal conductivities lead to lower temperatures. Lower temperatures lead to higher liquid

volume fractions in the cathode catalyst layer and also higher ionic conductivity. It can also be noticed that the current density remains almost the same for low through-plane thermal conductivities with increasing in-plane thermal conductivity for all voltages shown in Fig. 3.3a. As shown in Fig. 3.5, the higher in-plane thermal conductivities create more uniform temperatures than lower in-plane thermal conductivities. It can also be noticed in Fig. 3.5 that the maximum temperature is lower if the in-plane thermal conductivity of the GDL is high. Higher in-plane thermal conductivities thus reduce the risk of formation of hot spots in the region directly exposed to gas channel and also reduce the possibility of excessively low temperatures in the region directly in contact with the current collector. More uniform temperatures thus reduce the susceptibility of local dry-out of the ionic membrane in the region directly exposed to gas channel and also reduce the possibility of excessive liquid accumulation in the low temperature regions. Thus a combination of high in-plane thermal conductivity and a low through-plane thermal conductivity of the GDL yields higher current densities.

The effects of liquid water accumulation are more severe in regions further away from the inlet due to reduction in reactant concentration and a highly humidified cathode stream created by the product water joining the cathode gas channel. Hence in general, in order to maximize the current density under fully humidified inlet conditions, the through-plane thermal conductivity of the GDL should be as low as possible and the in-plane thermal conductivity should be as high as possible.

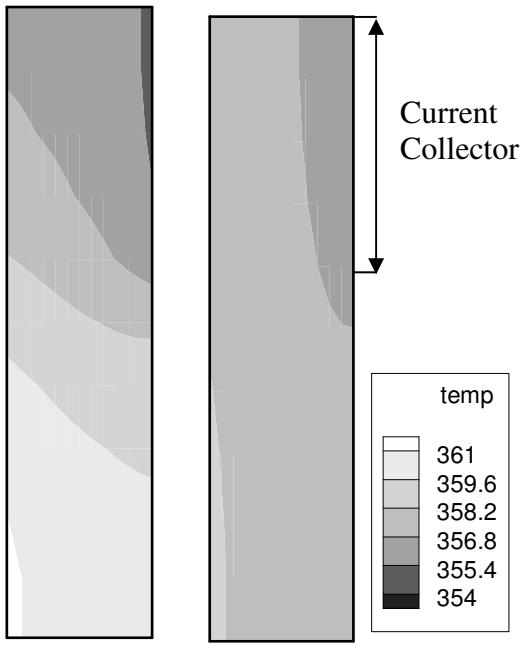

Fig. 3.5 Comparison of temperature distributions in the cathode GDL for low and high in-plane GDL thermal conductivities for fully humidified cathode inlet flow. (a) k_{xx} = 1.0 W $m^{-1}K^{-1}$ and k_{yy}/k_{xx} = 1.0; (b) k_{xx} = 1.0 W $m^{-1}K^{-1}$ and k_{yy}/k_{xx} = 10.

3.6.2 Low humidity cathode inlet

The effects of low humidity operation on current density, ionic conductivity and catalyst layer liquid volume fraction are shown in Figs. 3.6 and 3.7. We show the results at two different distances from the inlet. The ionic conductivity and liquid accumulation

in the catalyst layer are reduced due to the lower cathode humidity. However, the reduction in liquid accumulation in the cathode catalyst layer has a significant impact on current density and hence the current density increases with lower humidity. If the inlet cathode humidity is reduced below a certain value, the effect of lower ionic conductivity starts to dominate and the current density decreases. Thus, for low humidity operation, the region near the inlet may experience membrane dehydration while the regions away from the inlet generate higher current densities. Thus, even though low cathode humidity improves current densities away from the inlet, the adverse effect of membrane dehydration prevents the use of low cathode inlet humidities.

In order to address the problem of membrane dehydration near the inlet at low humidities, Dong et al. [60] suggested using a fully humidified anode inlet flow at a temperature above the fuel cell operating temperature. With an aim to develop an

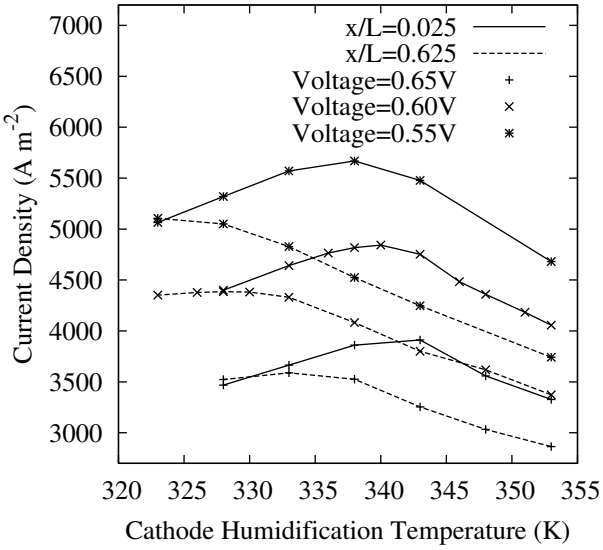

Fig. 3.6 Variation of current density with cathode humidification temperature at different distances from inlet.

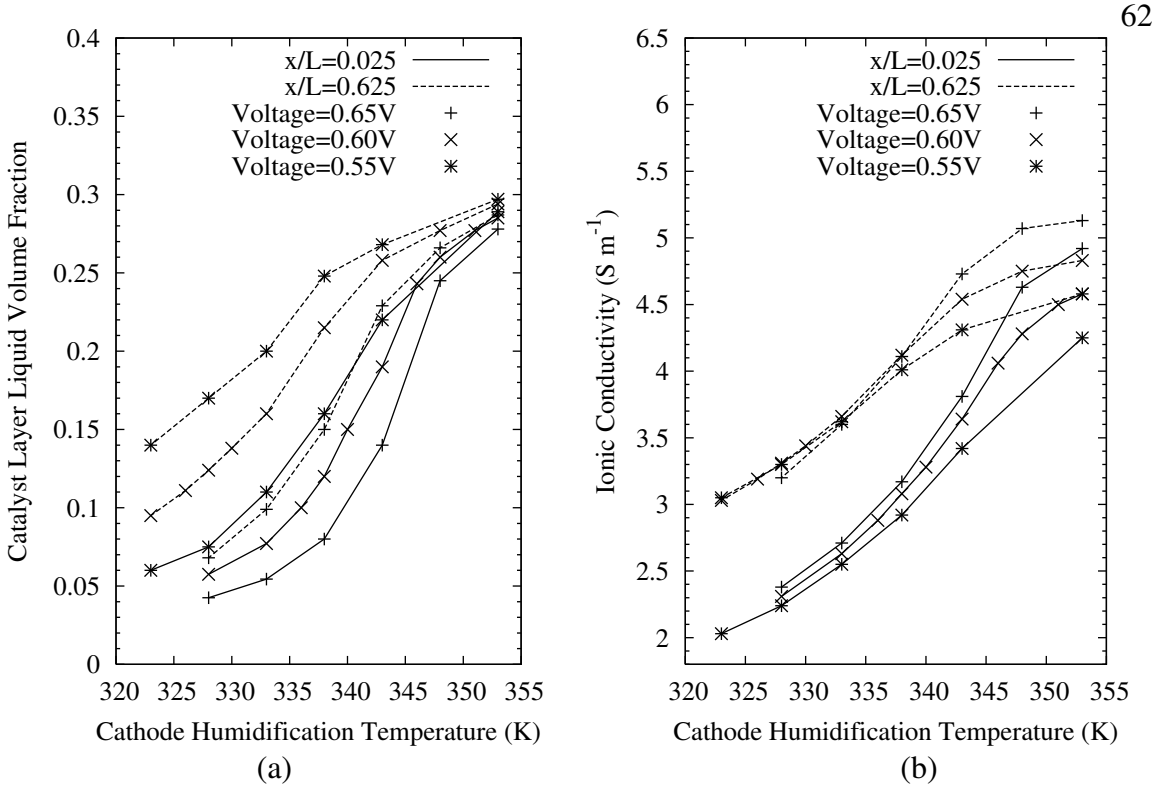

Fig. 3.7 Variation of (a) catalyst layer liquid volume fraction and (b) ionic conductivity with cathode humidification temperature at different distances from inlet.

alternative methodology to address the problem of membrane dehydration near the inlet, we now investigate the effect of GDL thermal conductivities on low humidity operation. Figure 3.8 shows the variation of current density near the inlet for different through-plane thermal conductivities at low humidities. Higher through-plane thermal conductivities result in higher current densities at lower cathode humidities. Higher through-plane thermal conductivities in conjunction with high in-plane thermal conductivities (see Table 3.3) result in lower and more uniform temperatures inside the fuel cell which in turn lead to a higher water vapor activity and hence reduce the risk of membrane dehydration near the inlet. At lower voltages, higher through-plane thermal conductivity leads to higher liquid accumulation in the cathode catalyst layer. Therefore, the maximum

current density at a given through-plane thermal conductivity occurs at a lower humidification temperature for lower voltages. The analysis presented in section 3.6.1 shows that high through-plane thermal conductivities promote liquid accumulation in the catalyst layer at fully humidified inlet conditions. The effect of liquid accumulation is more severe in regions away from the inlet because the cathode gas channel humidity increases towards the flow channel exit. Therefore, the current density can be increased

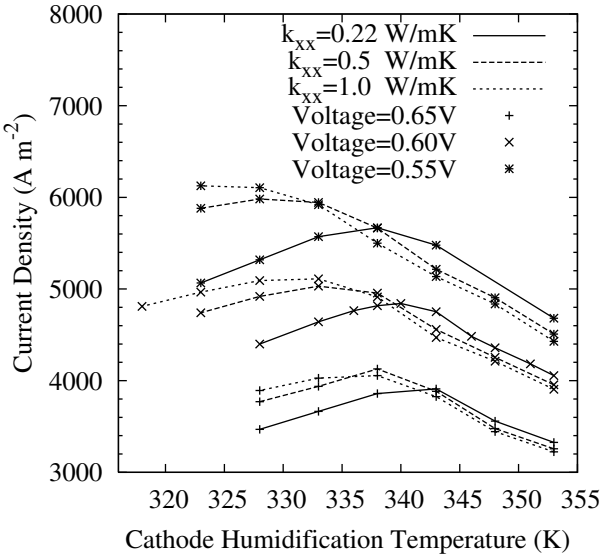

Fig. 3.8 Variation of current density with cathode humidification temperature near fuel cell inlet for different through-plane thermal conductivities of the GDL.

if membrane dehydration can be prevented near the inlet without allowing liquid water to accumulate in the region away from the inlet. The current density can thus be increased by constructing a GDL with a high through-plane thermal conductivity near the inlet of the flow channel and progressively lower through-plane thermal conductivity in regions away from the inlet. The through-plane thermal conductivity of the GDL at any distance from the inlet can be optimized to provide the maximum current density at a given

cathode humidity and operating voltage. The GDL can then be constructed to have these optimized thermal conductivities at appropriate distances along the flow channel to maximize the current density at the operating voltage. The through-plane thermal conductivity of the GDL can thus be tailored to reduce the susceptibility of membrane dehydration near inlet and also to reduce the risk of liquid accumulation in the catalyst layer in regions away from the inlet.

3.6.3 Effect of rib width

The effect of rib width variation on fuel cell operation has been analyzed previously [61-64] from the point of view of reducing the resistance to reactant diffusion and electron transport. Previously, [36] we used a single-phase model to analyze the effect of variation of rib width on temperature distribution inside a fuel cell. We showed that narrower ribs lead to higher temperatures and using GDLs with highly anisotropic thermal conductivity (higher in-plane thermal conductivity) leads to uniform and lower temperatures. We extend our analysis further in this work.

Figures 3.9 and 3.10 show the effect of variation of through-plane thermal conductivity on current density, ionic conductivity, maximum fuel cell temperature and cathode catalyst layer liquid accumulation for different rib widths. The results shown in Figs. 3.9 and 3.10 are for fully humidified cathode and anode flows near the inlet. Narrower ribs reduce the resistance to diffusion of water vapor from cathode catalyst layer to the gas channel. This reduction in water vapor diffusion resistance lowers the accumulation of liquid water in the cathode catalyst layer. Hence, for the voltages shown

in Figs. 3.9 and 3.10, smaller rib widths lead to higher current densities. Figure 3.10 also shows that the temperatures are higher for narrower ribs for all the considered voltages. Narrower ribs lead to higher temperatures, because higher current densities lead to more heat generation and smaller rib widths reduce the area of heat transfer from the GDL to the coolant channel. Also, the variation of current density with increasing through-plane thermal conductivity shows a maximum in case of small rib widths (rib:channel=1:5 in Fig. 3.9). Lower through-plane thermal conductivities lead to higher temperatures which reduce liquid accumulation in the cathode catalyst layer and also reduce the ionic conductivity of the membrane. In addition, as seen from Fig. 3.10, the accumulation of liquid water in the cathode catalyst layer is reduced for narrower ribs. In case of fuel cells using narrow ribs and GDLs with low through-plane thermal conductivities, the reduced membrane ionic conductivity has a larger negative impact on current density than the positive effect of reduction in cathode catalyst layer liquid accumulation. Therefore, for fuel cells using narrow ribs and operating at fully humidified inlet condition, the through-plane thermal conductivity should be maintained at a higher value in order to maximize the current density near the inlet. In regions further away form the inlet, the humidity of the cathode gas channel flow is higher and lower through-plane thermal conductivities can be used without adversely affecting the current density. Therefore, the methodology to tailor the GDL through-plane thermal conductivity proposed in section 3.6.2 can also be used to maximize the current density for fuel cells using narrow ribs and operating at fully humidified inlet conditions. In the present analysis, we have not considered the effect of reducing the rib width on electron transport [62] and also on the structural

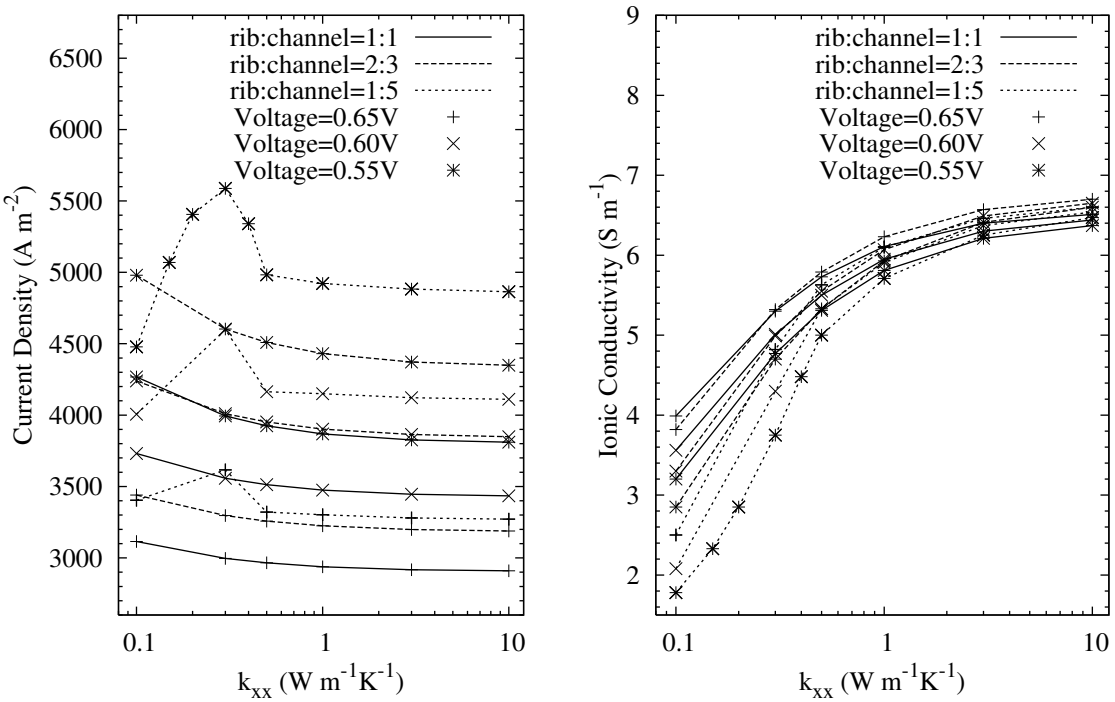

Fig. 3.9 Variation of (a) current density and (b) ionic conductivity with through-plane thermal conductivity of the GDL for different rib widths near inlet at fully humidified cathode inlet flow condition.

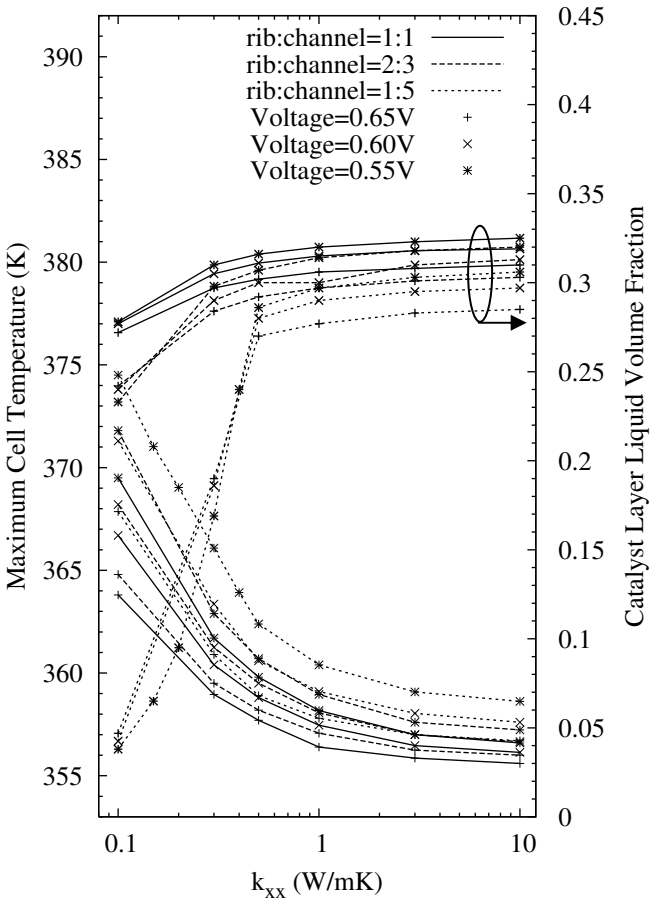

Fig. 3.10 Variation of maximum fuel cell temperature and catalyst layer liquid volume fraction with through-plane thermal conductivity of the GDL for different rib widths near the inlet at fully humidified cathode inlet flow condition.

strength of the current collector plate. The current density of the fuel cell operating at fully humidified inlet conditions is maximum if the current collector rib is as narrow as permitted by the structural strength and electron transport limitations.

Figure 3.11 shows the effect of rib width on low humidity operation near the inlet. Narrower ribs generate higher current densities even at lower cathode humidities by

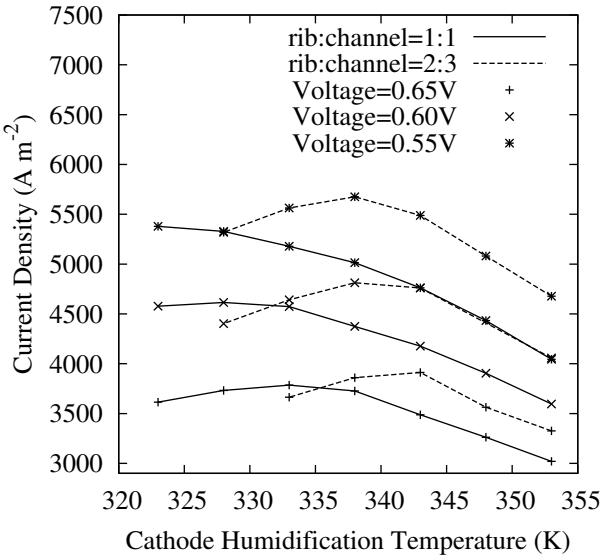

Fig. 3.11 Variation of current density with cathode humidification temperature near fuel cell inlet for different rib widths.

reducing the resistance to diffusion of gases through the GDL. However, at cathode humidities lower than an optimum value, wider ribs are able to generate higher current densities. Wider ribs are therefore more effective in reducing the susceptibility of membrane dehydration near the inlet. However, as discussed earlier in this section, narrower ribs promote the establishment of higher current densities at fully humidified inlet conditions. Hence it would be desirable to use wider ribs near the inlet and narrower ribs in the region away from the inlet in order to maximize the current density at low humidity operating conditions. The width of the ribs can thus be tailored to obtain maximum current density at a given voltage and given cathode inlet humidity.

3.7 Conclusions

A two-dimensional two-phase model is presented to predict the effect of GDL thermal conductivity on the polarization behavior under different operating conditions. The important conclusions from the study are summarized by:

1. The fuel cell generates high current densities with moderately high temperatures for a low value of through-plane thermal conductivity and a high in-plane thermal conductivity of the GDL.
2. By tailoring the GDL to have high through-plane thermal conductivity near the inlet, membrane dehydration may be avoided for low humidity operating conditions.
3. Similarly, the current density may be maximized at low humidity operating conditions by tailoring the GDL to have high through-plane thermal conductivity near the inlet and progressively decreasing through-plane thermal conductivity at distances farther away from the inlet along the flow channel.
4. Narrower current collector ribs lead to higher current densities for fuel cells using a fully humidified cathode inlet flow.
5. Near the inlet, fuel cells with wider ribs produce higher current density than those with narrower ribs if the cathode inlet humidity is below a certain value.

6. The current density can be maximized at lower cathode inlet humidities by using wider ribs in the region near the inlet and narrower ribs in the region away form the inlet.

The model presented in this chapter accounts for the effects of two-phase transport on fuel cell operation. However, it does not account for the effects of anisotropic electrical resistivity of the GDLs. We analyze these effects in the next chapter.

3.8 References

[1] Pasaogullari, U. and Wang, C. Y., 2004, *J. Electrochem. Soc.*, vol. 151, p. A399.

[2] Fuller, T. F. and Newman, J., 1995, *J. Electrochem. Soc.*, vol. 140, p. 1218.

[3] Nguyen, T. V. and White, R. E., 1993, *J. Electrochem. Soc.*, vol. 140, p. 2178.

[4] Baschuk, J. J. and Li, X., 2000, *J. Power Sources*, vol. 86, p. 181.

[5] Sukkee, U. and Wang, C. Y. and Chen, K. S., 2000, *J. Electrochem. Soc.* vol. 147, p. 4485.

[6] Gurau, V., Liu, H. and Kakac, S., 1998, *AICHE J.*, vol. 44, p. 2410.

[7] Meng, H. and Wang, C. Y., 2005, *J. Electrochem. Soc.*, vol. 152, p. A1733.

[8] Stockie, J. B., 2002, *Proceedings of IMECE'02, 2002 ASME International Mechanical Engineering Congress and Exposition*, HTD-Vol. 7, p. 393.

[9] Berning, T. and Djilali, N., 2003, *J. Electrochem. Soc.*, vol. 150, p. A1589.

[10] Wang, Z. H., Wang, C. Y. and Chen, K. S., 2001, *J. Power Sources*, vol. 94, p. 40.

[11] Natarajan, D. and Nguyen, T. V., 2001, *J. Electrochem. Soc.*, vol. 148, p. A1324.

[12] Hu, M., Gu, A., Wang, M., Zhu, X. and Yu, L., 2004, *Energy Convers. Manage.*, vol. 45, p. 1861.

[13] Hu, M., Gu, A., Wang, M., Zhu, X. and Yu, L., 2004, *Energy Convers. Manage.*, vol. 45, p. 1883.

[14] Mazumder, S. and Cole, J. V., 2003, *J. Electrochem. Soc.*, vol. 150, p. A1510.

[15] Sun, H., Liu, H. and Guo, L., 2005, *J. Power Sources*, vol. 143, p. 125.

[16] Birgersson, E., Noponen, M. and Vynnycky, M., 2005, *J. Electrochem. Soc.*, vol. 152, p. A1021.

[17] Baschuk, J. J. and Li, X., 2004, *J. Power Sources*, vol. 142, p. 134.

[18] Shimpalee, S., Greenway, S., Spuckler, D. and Van Zee, J. W., 2004, *J. Power Sources*, vol. 135, p. 79.

[19] Meng, H. and Wang, C. Y., 2005, *Fuel Cells*, vol. 5, p. 455.

[20] Meng, H., 2007, *J. Power Sources*, vol. 168, p. 218.

[21] Wang, C. Y. and Cheng, P., 1997, *Adv. Heat Transfer*, vol. 30, p. 93.

[22] Wang, C. Y., and Cheng, P., 1996, *Int. J. Heat Mass Transfer*, vol. 39, p. 3607.

[23] Meng, H., 2006, *J. Power Sources*, vol. 162, p. 426.

[24] Weber, A. Z. and Newman, J., 2003, *J. Electrochem. Soc.*, vol. 150, p. A1008.

[25] Weber, A. Z. and Newman, J., 2004, *J. Electrochem. Soc.*, vol. 151, p. A311.

[26] Ju, H., Meng, H. and Wang, C. Y., 2005, *Int. J. Heat Mass Transfer*, vol. 48, p. 1303.

[27] Benziger, J., Nehlsen, J., Blackwell, D., Brennan, T. and Itescu, J., 2005, *J. Membrane Sc.*, vol. 261, p. 98.

[28] Kurabayashi, K., 2001, *Int. J. Thermophysics*, vol. 12, p. 277.

[29] Hansen, D. and Bernier, G. A., 1972, *Poly. Eng. Sci.*, vol. 12, p. 204.

[30] Morelli, D. T., Heremans, J., Sakomoto, M. and Uher, C., 1986, *Phys. Rev. Letters*, vol. 57, p. 869.

[31] Kurabayashi, K., Asheghi, M., Touzelbaev, M. and Goodson, K. E., 1999, *IEEE J. Microelectro. Sys.*, vol. 8, p. 180.

[32] Toray Industries Inc. GDL specification sheet.

[33] Mathias, M., Roth, J. and Fleming, J. and Lehnert, W., 2003, *Handbook of Fuel Cells – Fundamentals, Technology and Applications, Volume 3: Fuel Cell Technology and Applications*, John Wiley & Sons, Ltd., Chichester, England, 2003, pp. 517.

[34] Pasaogullari, U., Mukherjee, P. P., Wang, C. Y. and Chen, K. S., 2006, *ECS Trans.*, vol. 3, p. 1239.

[35] Pharoah, J. G., Karan, K. and Sun, W., 2006, *J. Power Sources*, vol. 161, p. 214.

[36] Bapat, C. J. and Thynell, S. T., 2007, *J. Heat Transfer*, vol. 129, p. 1109.

[37] Ishii, M., *Thermo-Fluid Dynamic Theory of Two-Phase Flow*, Eyrolles, Paris, 1975.

[38] Drew, D. A. and Passman, S. L., 1999, *Theory of Multicomponent Fluids*, Springer-Verlag, New York, NY, 1999.

[39] Hassanizadeh, M. and Gray, W. G., 1979, *Adv. Wat. Res.*, vol., p. 131.

[40] Hassanizadeh, M. and Gray, W. G., 1979, *Adv. Wat. Res.*, vol. 2, p. 191.

[41] Bernardi D. M. and Verbrugge M. W., 1992, *J. Electrochem. Soc.*, vol. 139, p. 2477.

[42] Fox, R. W. and McDonald, A. T., 2001, *Introduction to Fluid Mechanics*, John-Wiley and Sons, New York, NY.

[43] Weber, A. Z. and Newman, J., 2004, *J. Electrochem. Soc.*, vol. 151, p. A326.

[44] Culligan, K. A., Wildenschild, D., Christensen, B. S. B., Gray, W. G., Rivers, M. L. and Tompson, A. F. B., 2004, *Wat. Resources Res.*, vol. 40, p. W12413.

[45] Held, R. J. and Celia, M. A., 2001, *Adv. Wat. Res.*, vol. 24, p. 325.

[46] Reeves, P. C. and Celia, M. A., 1996, *Wat. Resources Res.*, vol. 32, p. 2345.

[47] Rivin, D., Kendrick, C. E., Gibson, P. W. and Schneider, N. S., 2001, *Polymer*, vol. 42, p. 623.

[48] Gostick, J. T., Fowler, M. W., Ioannidis, M. A., Pritzker, M. D., Volfkovich, Y. M. and Sakars, A., 2006, *J. Power Sources*, vol.156, p. 375.

[49] Benziger, J., Nehlsen, J., Blackwell, D., Brennan, T. and Itescu, J., 2005, *J. Membrane Sci.*, vol. 261, p. 98.

[50] Khandelwal, M. and Mench, M. M., 2006, *J. Power Sources*, vol. 161, p. 1106.

[51] Hinatsu, J. T., Mizuhata, M. and Takenaka, H., 1994, *J. Electrochem. Soc.*, vol. 141, p. 1493.

[52] Parthasarathy, A., Srinivasan, S. and Appleby, J. A., 1992, *J. Electrochem. Soc.*, vol. 139, p. 2530.

[53] Shah, R. K. and London, A. L., 1978, *Laminar Flow Forced Convection in Ducts*, Academic Press, New York.

[54] Patankar, S. V., 1980, *Numerical Heat Transfer and Fluid Flow*, Hemisphere, Washington, D.C.

[55] Mench, M. M., Wang, C. Y. and Ishikawa, M., 2003, *J. Electrochem. Soc.*, vol. 150, p. A1052.

[56] Hollinger, A., 2006, *Contact Resistance Measurements of Gas-diffusion layers and Membrane for Fuel Cell Applications*, Senior Honors Thesis, Department of Engineering Science and Mechanics, The Pennsylvania State University, University Park, PA.

[57] Cussler, E. L., 1976, *Multicomponent Diffusion*, Elsevier Scientific Pub. Co., Amsterdam, New York.

[58] T.A. Zawodzinski, T. A., Dawy, J., Valerio, J. and Gottesfeld, S., 1995, *Electrochimica Acta*, vol. 40, p. 297.

[59] Zhang, J., Xie, Z., Zhang, J., Tang, Y., Song, C., Navessin, T., Shi, Z., Song, D., Wang, H., Wilkinson, D. P., Liu, Z. S. and Holdcroft, S., 2006, *J. Power Sources*, vol.160, p. 872.

[60] Dong, Q., Mench, M. M., Cleghorn, S. and Beuscher, U., 2005, *J. Electrochem. Soc.*, vol. 152, p. A2114.

[61] Jeng, K. T., Lee, S. F., Tsai, G. F. and Wang, C. H., 2004, *J. Power Sources*, vol. 138, p. 41.

[62] Senn, S. M. and Poulikakos, D., 2005, *J. Heat Transfer*, vol. 127, p. 1245.

[63] Berning, T. and Djilali, N., 2003, *J. Power Sources*, vol. 124, p. 440.

[64] Grigoriev, S. A., Kalinnikov, A. A., Fateev, V. N. and Wragg, A. A., 2006, *J. Appl. Electrochem.*, vol. 36, p. 191.

Chapter 4

Effect of anisotropic electrical resistivity

4.1 Introduction

The effect of an isotropic electrical conductivity of the GDL on fuel cell operation was analyzed by Senn and Poulikakos [1] using a two-dimensional non-isothermal model and by Meng and Wang [2] using a three-dimensional isothermal model. The GDLs are commonly constructed of carbon fibers either in woven or paper form. Electron micrographs for different GDLs [3] suggest that the carbon fibers are preferentially oriented in the in-plane direction. Also, the thermal and electrical conductivity measurements for certain GDLs [4, 5] reveal a high degree of anisotropy. The effect of anisotropic electrical conductivity of the GDLs on the reaction rate in the cathode catalyst layer was analyzed by Sun et al. [6] using a single-phase, isothermal model. In the previous chapter, we provided a comprehensive analysis of the effects of an anisotropic thermal conductivity on heat and two-phase transport inside a fuel cell. In this chapter, we extend our analysis to examine the effects of an anisotropic electrical resistivity of the GDLs on current density and temperature distribution by further refining the two-dimensional, two-phase model presented in Chapter 3.

4.2 Model formulation

The model used in this work accounts for the non-uniform nature of the two-phase flow of reactants, products and ionic species, as well as the generation and transport of heat. The two-dimensional computational domain used in our work is shown in Fig. 1.1, along with a cross-section showing flow channels, GDLs and the membrane in a PEMFC. A detailed description of model formulation, constitutive equations and boundary conditions can be found in the previous chapter is sections 3.2, 3.3 and 3.4 respectively. In addition to the model equations described in the previously, we apply

$$\nabla \cdot \left(\boldsymbol{\sigma}^{-1} \cdot \nabla \phi_s \right) = j \tag{4.1}$$

to solve for the solid-phase potentials in the catalyst layers and GDLs. The boundary conditions at the interfaces of membrane/catalyst layer, anode GDL/bipolar plate and cathode GDL/bipolar plate interface are, respectively, given by

$$\nabla \phi_s = 0 \tag{4.2a}$$

$$\phi_s = U_0 - V_{cell} \tag{4.2b}$$

$$\phi_s = 0 \tag{4.2c}$$

A detailed description of the source terms j, model validation, baseline parameter values and numerical scheme can be found in Table 3.1 and section 3.5 respectively.

4.3 Discussion of results

The typical values for the in-plane and through-plane electrical resistivities of GDLs are 5.8×E-5 Ω m and 80×E-5 Ω m, respectively [4]. Thus, the electrical

resistivities of the GDLs are highly anisotropic and low in magnitude. Thus, the GDLs are very good electrical conductors. In this chapter, we present a parametric analysis of the possible effects of variation of electrical resistivities on the current density and temperature distribution in a fuel cell. Also, in this chapter the term 'average current density' to refers to the current density averaged over the total active area of fuel cell.

4.3.1 Effect on current density

The effect of variation of in-plane electrical resistivity of the GDL on current density is shown in Fig. 4.1 for a low value of through-plane resistivity of the GDL.

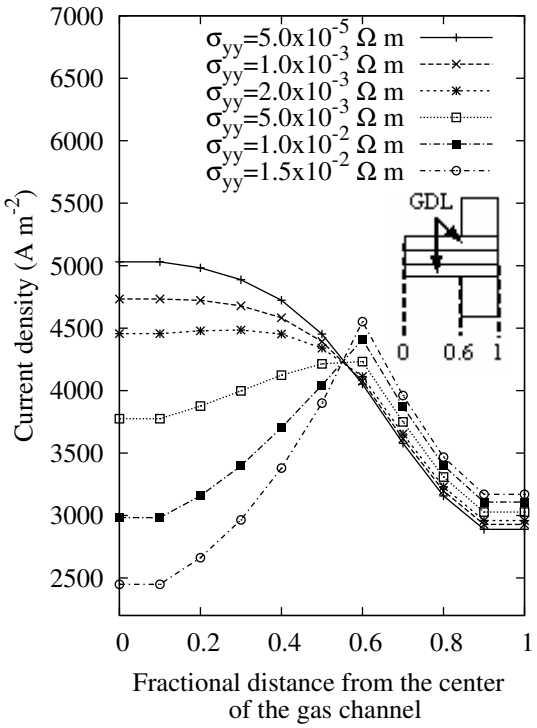

Fig. 4.1 Variation of local current density with in-plane electrical resistivity, with a through-plane resistivity of $5.0x10^{-5}\,\Omega\,m$.

As expected, the average current density reduces with increasing in-plane electrical resistivity of the GDL. Figure 4.1 also shows that, in the region directly exposed to the gas channel, the local current density decreases significantly with increasing in-plane resistivity of the GDL. However, the local current density increases by a small amount in the region adjacent to the current collector. This variation of the current density can be better explained with the help of Fig. 4.2, which shows the possible paths for transport

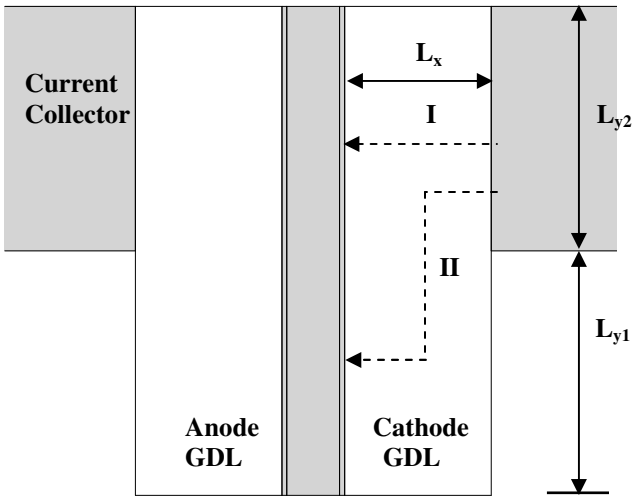

Fig. 4.2 Schematic representation of transport of electrons in a GDL.

of electrons from the current collector to the cathode catalyst layer. The electrical resistances for both these paths can be approximately expressed by

$$R_I = \sigma_{xx} \frac{L_x}{L_{y2}} \tag{4.3a}$$

$$R_{II} = \sigma_{xx} \frac{L_x}{2} \left(\frac{1}{L_{y1}} + \frac{1}{L_{y2}} \right) + \sigma_{yy} \frac{\left(L_{y1} + L_{y2} \right)}{2L_x} \tag{4.3b}$$

Equation 4.3b reveals that the in-plane electrical resistivity of the GDL adversely affects the transport of electrons from the current collector to the region of cathode catalyst layer exposed to the gas channel, shown by path II in Fig. 4.2.

In the region of the GDL adjacent to the current collector, the electrons are transported along the path I in Fig. 4.2. Hence, as seen from Eq. 4.3a, variation in the in-plane electrical resistivity of the GDL does not directly affect the current density in this region. However, in the region directly exposed to gas channel, the local current density and hence the local rate of electrochemical reaction decreases with increasing in-plane resistivity. This decrease in the electrochemical reaction rate leads to increased concentration of reactants in the region adjacent to the current collector. Therefore the local current density slightly increases in the region adjacent to the current collector.

The effect of varying the through-plane electrical resistivity of the GDL on current density is shown in Fig. 4.3. Again, the average current density decreases with increasing through-plane electrical resistivity. Equations 4.3a and 4.3b show that the through-plane electrical resistivity affects the transport of electrons from the current collector to the entire catalyst layer. Hence the local current density decreases with increasing through-plane resistivity of the GDL for the entire catalyst layer.

4.3.2 Effect on catalyst layer temperatures

It has been shown previously that the maximum temperature in a fuel cell occurs in the cathode catalyst layer [7]. The local temperature in the cathode catalyst layer

depends on the kinetic losses, ohmic heat generation and also on reversible heat generation. The electrochemical reaction rate depends on the

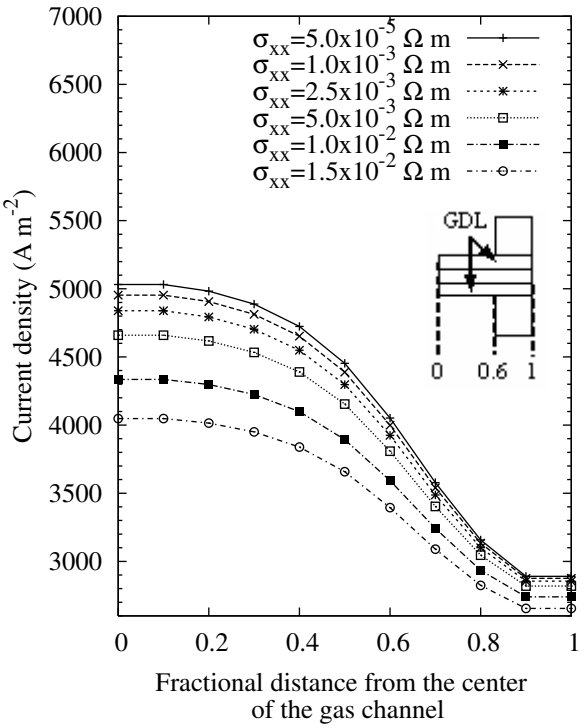

Fig. 4.3 Variation of local current density with through-plane electrical resistivity, with an in-plane resistivity of $5.0x10^{-5}\,\Omega\,m$.

overpotential, temperature in the catalyst layer, concentration of the reactants and liquid accumulation in the catalyst layer. Lower reaction rate reduces heat generation rate and hence the local temperature in the catalyst layer. Lower temperatures reduce the electrochemical reaction rate even further by reducing the exchange current density [8] and by allowing more liquid accumulation. In addition, the ohmic heat generation rate depends on the local current density and the reversible heat generation rate depends on the local temperature. The temperature distribution in the catalyst layer is also affected by

the thermal conductivity of the GDL. Thus the local temperature in the catalyst layer is determined by the relative contributions of all these competing factors.

The effects of varying the in-plane and through-plane electrical resistivity of the GDL on temperature distribution in the cathode catalyst layer are shown in Figs. 4.4 and 4.5. As expected, the positions of maximum local current density in Figs. 4.1 and 4.3 coincide with the positions of maximum local temperature in Figs. 4.4 and 4.5. Thus the local current density and hence the local electrochemical reaction rate are the factors determining the location of maximum temperature in a fuel cell. However, as shown in Fig. 4.4, in the region adjacent to the current collector, the local temperatures decrease even though the local current density increases with increasing in-plane resistivity of the GDL as shown in Fig. 4.1. Figures 4.3 and 4.5 show that the change in local current density with increasing through-plane resistivity is larger in the region exposed to gas channel than in the region adjacent to the current collector. However, the change in the local temperature in the catalyst layer with increasing through-plane resistivity is nearly constant for the entire catalyst layer. Thus, in the region adjacent to the current collector, the local current density is not the dominant factor for determining the local temperature in the cathode catalyst layer. We have shown in the previous chapters that using GDLs with highly anisotropic thermal conductivity unifies the temperature distribution. Such a temperature distribution leads to lower maximum temperature and higher minimum temperature in the cathode catalyst layer. Thus, in case of GDLs with highly anisotropic thermal conductivities, the minimum temperature in the catalyst layer is governed by the in-plane thermal conductivity of the GDL. It can be noticed from Figs. 4.1, 4.3, 4.4 and 4.5 that both maximum and minimum temperatures in the catalyst layer decrease

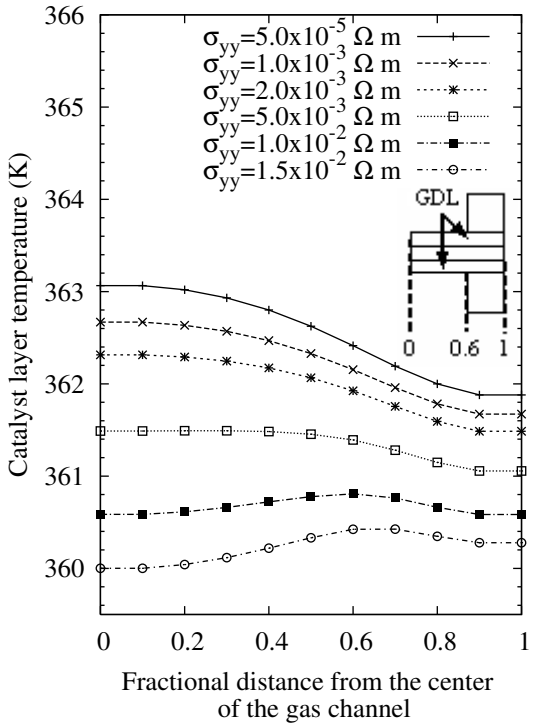

Fig. 4.4 Variation of catalyst layer local temperature with in-plane electrical resistivity, with a through-plane resistivity of $5.0x10^{-5}\,\Omega\,m$.

with decreasing average current densities even though in some cases the maximum local current densities increase with decreasing average current densities. Thus, for GDLs with high in-plane thermal conductivities, the maximum and minimum temperatures in the cathode catalyst layer depend on the average current density rather than the local current density in the catalyst layer.

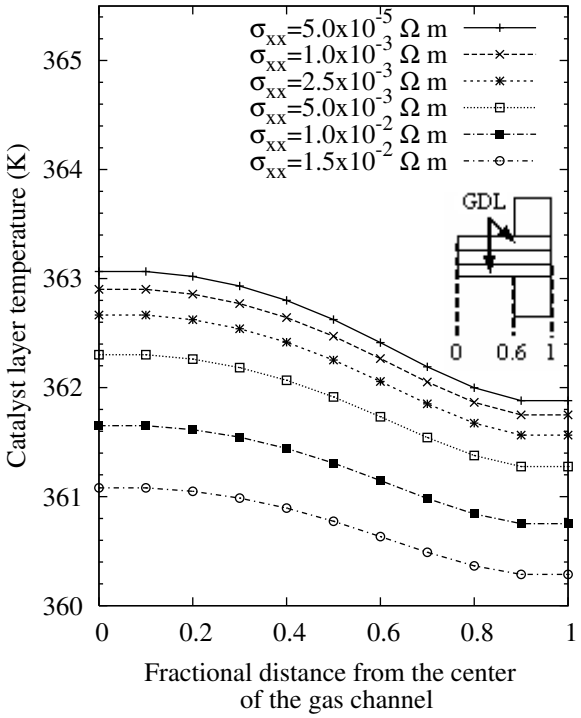

Fig. 4.5 Variation of catalyst layer local temperature with through-plane electrical resistivity for an in-plane resistivity of $5.0x10^{-5}\,\Omega\,m$.

4.4 Conclusions

A two-dimensional two-phase, non-isothermal model developed previously has been extended to account for an anisotropic electrical conductivity of the GDL. The important conclusions from the study are summarized by:

1. In the region directly exposed to the gas channel, local current density decreases with increasing in-plane GDL electrical resistivity.
2. A higher in-plane GDL electrical resistivity results in a slightly higher local current density in the region directly in contact with the current collector.

3. The local current density decreases with increasing through-plane resistivity of the GDL for the entire catalyst layer. The effect is more severe in the region of the catalyst layer directly exposed to the gas channel.
4. The maximum and minimum temperatures in the cathode catalyst layer are largely governed by the average current density rather than the local current density for a GDL with a highly anisotropic thermal conductivity.

This completes our analysis of the steady-state operation of the fuel cell. In the next chapter, we use a three-dimensional model to analyze different heating techniques used for achieving a rapid startup of a fuel cell.

4.5 References

[1] Senn, S. M. and Poulikakos, D., 2005, *J. Heat Transfer*, vol. 127, p. 1245.

[2] Meng, H. and Wang, C. Y., 2004, *J. Electrochem. Soc.*, vol. 151, p. A358.

[3] Benziger, J., Nehlsen, J., Blackwell, D., Brennan, T. and Itescu, J., 2005, *J. Membrane Sc.*, vol. 261, p. 98.

[4] Toray Industries Inc. GDL specification sheet.

[5] Mathias, M., Roth, J., Fleming, J. and Lehnert, W., 2003, *Handbook of Fuel Cells – Fundamentals, Technology and Applications, Volume 3: Fuel Cell Technology and Applications*, John Wiley & Sons, Ltd., Chichester, England.

[6] Sun, W., Peppley, B. A. and Karan, K., 2005, *J. Power Sources*, vol. 144, p. 42.

[7] Khandelwal, M. and Mench, M. M., 2006, *J. Power Sources*, vol. 161, p. 1106.

[8] Parthasarathy, A., Srinivasan, S. and Appleby, J. A., 1992, *J. Electrochem. Soc.*, vol. 139, p. 2530.

Chapter 5

Comparative evaluation of heating techniques for room temperature startup of a PEMFC

5.1 Introduction

The polymer electrolyte membrane fuel cell (PEMFC) is being investigated as a possible replacement for the internal combustion engines in automobiles. In order to be considered a viable power source for automobiles, the ability of a PEMFC to start rapidly from low temperatures is of paramount importance. Although the operating temperatures for a PEMFC are in the range of 60-80°C, the temperatures at the time of startup can range from sub-zero to room temperature. Therefore, the temperature of the fuel cell has to be raised to a value at which the electrochemical reaction rate is sufficiently high. Recently many experimental and numerical investigations [1-17] have studied the startup of a PEMFC at sub-zero temperatures. The effect of heating on startup of a PEMFC stack has also been studied [10, 18]. We present a comparative analysis of the techniques used to heat a single fuel cell from startup condition to a temperature close to the operating temperature. We use a three-dimensional numerical model for this purpose. We also study the effect of different parameters on these heating techniques.

5.2 Model formulation

The three-dimensional symmetrical section considered for the startup analysis is shown in Fig. 5.1. Serpentine gas channels are assumed, which have been used in

previously published experimental and numerical investigations of fuel cell operating behavior [19-21]. Thus, the assumption of serpentine gas channels is in line with the current trends in fuel cell technology. However, there is very little published data on the exact shape and size of liquid channels used in fuel cell stacks. The liquid channels, however, can be either serpentine or parallel. For the same total flow rate, the serpentine channels will show a larger pressure drop than the parallel channels. The choice of a particular liquid channel shape and size will depend on many other design requirements for a fuel cell stack. For the purposes of this work we assume parallel liquid channels. As shown in Fig. 5.1, we also assume the liquid and gas channels to have the same dimensions.

The gas-diffusion layers, the ionic membrane and the catalyst layers are porous in nature. We assume that the gases and the porous matrix are at local thermal equilibrium at each point inside these porous layers. Also, as the velocity of gases inside these porous structures is very low, we neglect the transport of heat due to flow of gases inside the GDLs, catalyst layers and the membrane. In addition, we consider the GDLs and catalyst layers to be completely dry at the time of startup. Hence, the effect of phase change is also neglected. Therefore, we use the conduction equation to analyze the transport of heat in the solid and porous structures in the fuel cell.

$$\frac{\partial}{\partial t}(\rho c_v T) = \nabla \cdot (\mathbf{k} \nabla T) + q''' \tag{5.1}$$

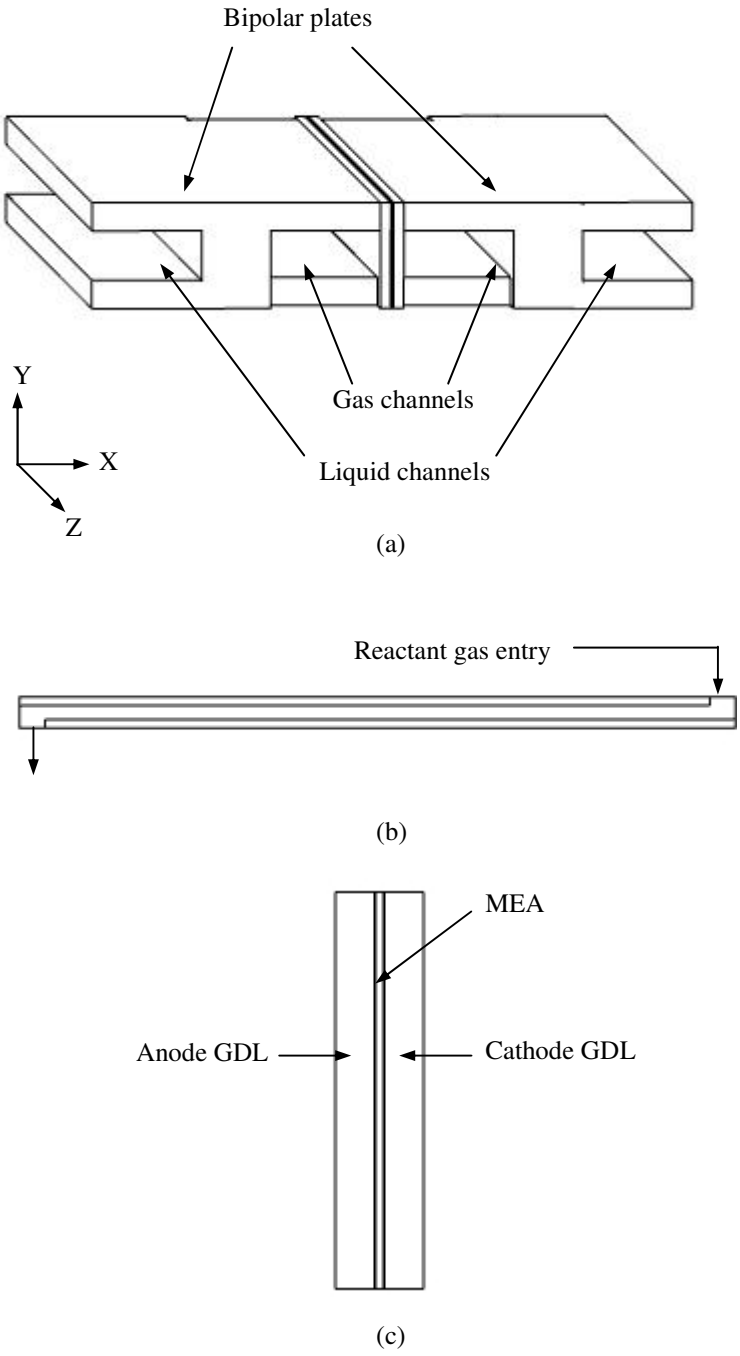

Fig. 5.1 The three-dimensional geometry used for numerical solution. (a) the complete 3d section, (b) section through the gas channels and (c) magnified view of x-y plane showing MEA and GDLs

The heat generation term in Eq. (5.1) may be set to zero depending on the heating technique being considered. The transport of heat in the gas and liquid channels is modeled using the energy conservation equation.

$$\frac{\partial}{\partial t}(\rho c_v T) + \nabla \cdot \left(\rho c_p \mathbf{v} T\right) = 0 \tag{5.2}$$

We neglect the effect of axial conduction and viscous dissipation in our work. Also, there is no heat generation in the gas and liquid channels.

The heat transfer at the channel/bipolar plate and channel/GDL interfaces occurs due to convection. All other faces in Fig. 5.1(a) are assumed to be insulated. The exact expressions for the heat transfer coefficients, heat sources and flow velocities required for the solution of Eqs. (5.1) and (5.2) depend on the specific heating technique considered. Hence we provide expressions these quantities for each case separately in the following sections. Also, we do not consider an operating fuel cell in our work.

5.3 Numerical solution

The porous and solid structures shown in Fig. 5.1(a) were divided into a three-dimensional block structured Cartesian grid. The temperatures were treated as cell-centered quantities. Equation 5.1 was discretized using second order accurate differences in space and first order accurate differences in time. The discretized equation was then solved using GMRES scheme [22].The flow channels were divided into a one-dimensional grid along the flow path. First-order upwind scheme was used to discretize the convective term. The grid size was chosen to ensure grid independence for both the

solid structures and channels. The solution was continued till the norm of the residual was below 10^{-4} at each time step.

5.4 Results and discussion

Numerical solution was obtained for different heating techniques using the method described in the previous section. We define the startup time as the time taken to raise the temperature in the MEA to at least 343.15 K everywhere. We assume the operating temperature of the fuel cell to be 353.15 K. Hence we heat the fuel cell to a temperature 10 K below the final operating temperature. We assume that, at this temperature, the waste heat from the electrochemical reactions is sufficient to further increase the temperature of the fuel cell to 353.15 K. However, there is some evidence to show that the electrochemical reactions may be self-sustaining at lower temperatures [9]. It should be noted that, as we do not include the effects of freezing of water and fuel cell operation in our model, the conclusions drawn in this chapter depend on the difference between the initial and final temperatures. Hence, as long as the fuel cell is free of ice and is not producing electrical power, the conclusions presented in this chapter are applicable even if the heating is started at sub-freezing temperatures. Additionally, for all the results shown in the following sections, except for the parameter values that are varied, all other parameters are kept at values given in Table 5.1.

Table 5.1. Model parameters

Parameter	Value
GDL thickness	300.0E-6 m
Catalyst layer thickness	10.0E-6 m
Membrane thickness	58.0E-6 m
Bipolar plate thickness	2.0E-3 m
Bipolar plate width: channel width	2:3
Channel length	7.1E-3 m
Total width of the symmetrical section	3.05E-3 m
Channel depth	3.0E-3 m
Bipolar plate specific heat	5.0E2 J/kg-K
GDL specific heat	681.0 J/kg-K
Catalyst layer specific heat	681.0 J/kg-K
Membrane specific heat	681.0 J/kg-K
Bipolar plate density	8.0E3 kg/m^3
GDL density	440.0 kg/m^3
Catalyst layer density	440.0 kg/m^3
Membrane density	440.0 kg/m^3
Bipolar plate thermal conductivity	16.0 W/m-K
GDL through-plane thermal conductivity	0.22 W/m-K
GDL in-plane thermal conductivity	22.0 W/m-K
Catalyst layer in-plane thermal conductivity	0.27 W/m-K

Membrane in-plane thermal conductivity	0.16 W/m-K
Ratio of thermal conductivities $k_{yy} : k_{xx}$ for GDL, membrane and catalyst layer	20 : 1
Thermal contact conductance	10.0 E3 W/m^{2}K
Initial temperature	303.15 K

5.4.1 Using hot fluids

The PEMFC can be heated by using hot liquid in the liquid channels or hot gas flow through the gas channels. We first analyze the effectiveness of hot liquids in heating the fuel cell. As seen from Table 5.1, the liquid channels have small sizes. Hence the flow in these channels is expected to be laminar. Further, the hydrodynamic and thermal entry lengths are relatively short compared to channel lengths. Hence, the convective heat transfer coefficients for the liquid channels are calculated using the following relation applicable for laminar fully developed flows in square channels [23]

$$Nu = \frac{hd_{hyd}}{k_f} = 2.98 \tag{5.3a}$$

where

$$d_{hyd} = \frac{4A_{cross}}{P} \tag{5.3b}$$

The hot water at 353.15 K is circulated through the liquid channels. There is no flow in the gas channels. The heat generation term in Eq. (5.1) is set to zero.

Figure 5.2 shows the effect of liquid flow rate on the startup time. The startup time for the fuel cell decreases with increasing liquid flow rate. Figure 5.1 shows that the liquid channels are parallel and straight. Hence lower flow rate increases the time required to heat the regions of the fuel cell farther away from the hot liquid inlet. Thus shorter channels will lead to lower startup times at lower liquid flow rates.

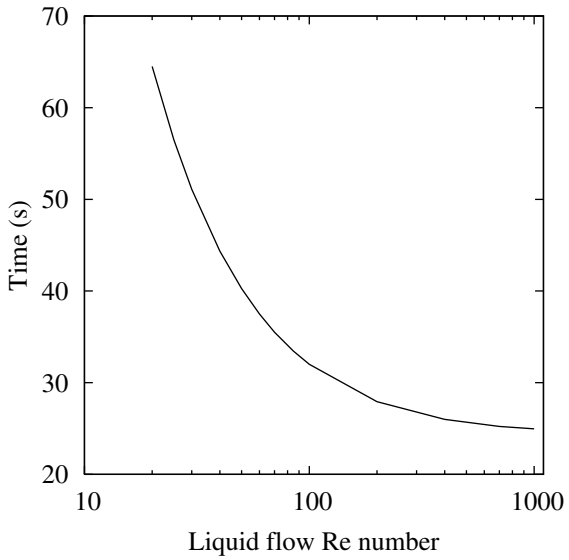

Fig. 5.2 Effect of hot liquid flow rate on startup time.

Figure 5.2 also shows that the reduction in startup time achieved by increasing the liquid flow rate reduces with increasing flow rate. As the liquid flow rate increases, the temperature of the hot liquid at the liquid channel exit increases which in turn reduces startup time. However, as the liquid temperature at the channel exit approaches a value close to the liquid temperature at the inlet, startup time cannot be reduced further by increasing the hot liquid flow rate. Also, the pressure drop for laminar flow in a channel is given by the Darcy law [24]

$$\Delta P = 32 \frac{\mu l v}{d_{hyd}^2} \tag{5.4}$$

Thus the pressure drop increases with increasing velocity of flow. Thus, a high rate of flow for the hot liquid may not result in a significant decrease in the startup time while increasing the pressure drop.

Equation 5.3 shows that the Nusselt number for laminar flow does not depend on the flow rate. However, the convective heat transfer can be enhanced using other techniques [25]. Figure 5.3 shows that the startup time decreases if the convective heat transfer is enhanced in the liquid channel. Figure 5.3 also shows that the dependence of the startup time on the heat transfer coefficient in the channels is almost linear. Thus, the thermal resistance at the liquid/bipolar plate interface is the dominant thermal transport parameter affecting the startup time and hence other thermal transport parameters have a very limited impact on startup time.

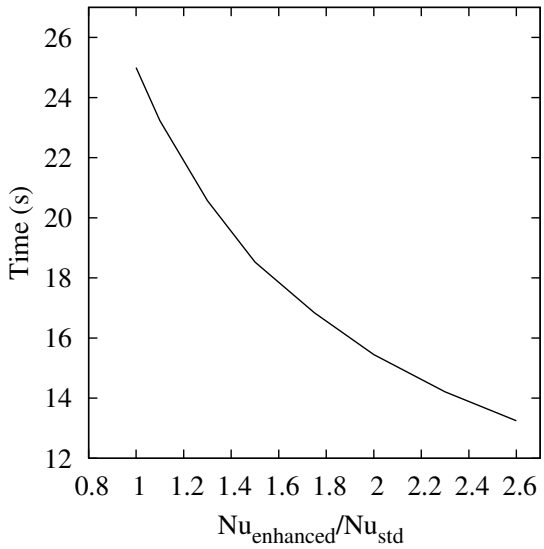

Fig. 5.3 Effect of liquid channel Nusselt number on startup time. Liquid Re = 1000.

The effect of bipolar plate size on fuel cell startup time is shown in Fig. 5.4. The term reference thickness in Fig. 5.4 refers to the thickness of the bipolar plate given in

Table 5.1. Increasing the thickness of the bipolar plates and width of the bipolar plate ribs increase the thermal mass of the bipolar plate and thus the startup time. However, increasing the width of the bipolar plate ribs also increases the area of heat transfer between the GDLs and the bipolar plate. This increase in area increases the rate of heat transfer to the MEA. However, increased bipolar plate thermal mass dominates and hence the startup time increases. Also, the slope of both curves in Fig. 5.4 is almost the same. Thus the positive effect of improved heat transfer at the GDL/bipolar plate interface is extremely small. This is expected because the dominant resistance for heat transport is the thermal resistance at the liquid/bipolar plate interface. Hence reducing any other thermal resistance does not affect the startup time for the fuel cell. Varying the thermal conductivities of GDLs and membrane also has a very limited impact on the startup time for the same reason.

Figure 5.4 also shows that the dependence of the startup time on the bipolar plate thermal mass is almost linear. Thus the startup time for the fuel cell can also be reduced by using bipolar plates made with materials with lower thermal mass and high thermal conductivities (e.g. graphite, foams etc.).

Further reduction in the startup time can be achieved by using flow of hot gases in the gas channels. Our previous discussion in this section shows that the startup time is dependent on the convective heat transfer coefficient at the channel/bipolar plate interface for liquid channel flows. The thermal conductivity of air is an order of magnitude lower than water. Hence, the convective heat transfer coefficient in the gas channel is an order of magnitude lower than that for the liquid channels. Hence the startup time would be

much higher if one were to use only a flow of hot gases in the gas channels to heat the fuel cell.

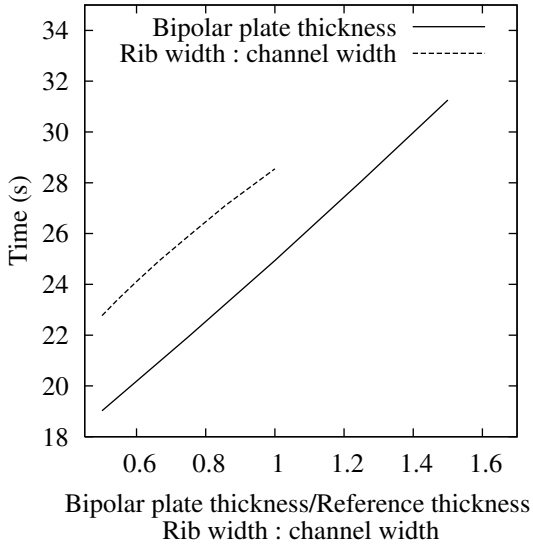

Fig. 5.4 Effect of bipolar plate size on startup time. Liquid *Re* = 1000.

5.4.2 Using electric heaters

We have seen in the earlier section that if hot fluids are used to heat fuel cell, the startup time depends on the *Re* number of flow and the convective heat transfer coefficient in the channels. The fuel cell can also be heated using electric heaters embedded in the bipolar plates. The required current can be supplied using an external battery. Such a heating technique would eliminate the need for power to drive a pump or compressor.

The most commonly used electric heater for fuel cell heating applications is the cartridge heater [26]. The cartridge heaters are available in different ratings and sizes [27] and generally give reliable performance even for high-temperature applications. However,

these heaters have some disadvantages when used for fuel cell heating applications. The cartridge heaters are at least a few millimeters in diameter and hence need a bored hole of that size in the bipolar plate. This requirement increases the thickness of the bipolar plate which in turn increases the startup time (see previous section). Also, as the cartridge heater and the bipolar plate are hard materials, the thermal contact conductance at this interface is expected to be low [28]. Such low thermal contact conductance can adversely affect the heat transfer rate from the heater to the fuel cell and can lead to higher fuel cell startup times. However, thin, flexible and planar electric heaters are also available [29, 30]. These heaters are generally used for heating applications at moderately high temperatures up to 200°C. As the operating temperatures for a fuel cell fall within this range, these heaters are ideally suited for fuel cell heating applications. These heaters are approximately 250 μm thick. This allows the use of thin bipolar plates. The thermal contact conductance at the heater/bipolar plate interface can also be expected to be high due to the softness of the external surface of the heater [31-33]. We assume that the heaters are embedded into the bipolar plates as shown in Fig. 5.5. The heaters are coated with polymer insulation. Thus, the position of the heaters as shown in Fig. 5.5 divides each bipolar plate into two parts that are electrically disconnected from each other. We assume that the two parts of each bipolar plate are electrically connected to each other using some other method. We do not go into the details of such methods in this chapter.

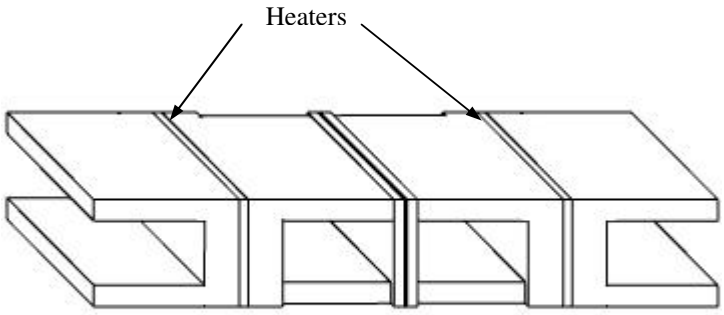

Fig. 5.5 Location of electric heaters in fuel cell.

We assume that the gas and liquid channels are filled with air at room temperature at the time of startup. The source term in Eq. (5.1) is used to account for the heat generation in the heater. We also assume that the density and specific heat capacity of the heaters is same as that of the bipolar plates because the heating element is expected to be metallic with properties similar to the bipolar plates. We also assume the thermal contact conductance at the GDL/bipolar plate interface and at the heater/bipolar plate interface to be equal. Both these contacts are between a metal and a thin, flexible material and are known to vary in the same range with applied pressure [34, 35, 31]. The effect of heater watt rating on startup time and heater temperature is shown in Fig. 5.6. The startup time can also be calculated using a lumped analysis

$$t = \frac{mc\Delta T}{W} \tag{5.5}$$

Figure 5.6 shows that the startup time can be very accurately estimated by the lumped analysis given by Eq. (5.5). Also, the heater temperature is within the rated temperature range for such heaters.

Figure 5.7 shows that low thermal contact conductance can increase startup time and heater temperature. However, it is important to notice the difference between Figs. 5.3 and 5.7. Figures 5.3 and 5.7 show that the startup time increases if the heat transfer coefficient at the interface between the source of heat (hot fluid in Fig. 5.3 and heater in Fig. 5.7) and the bipolar plates is reduced. However, while the temperature of the hot fluid is constant in Fig. 5.3, the temperature of the heater is allowed to increase. This rise in heater temperature compensates for the reduction in thermal contact conductance and helps to maintain the rate of heat transfer to the bipolar plate. However, as it takes more time to raise the temperature of the heater to a higher value, the startup time increases. The startup time also increases because the rate of heat transfer from the bipolar plate to the MEA is adversely affected by the reduction in the thermal contact conductance at the GDL/bipolar plate interface.

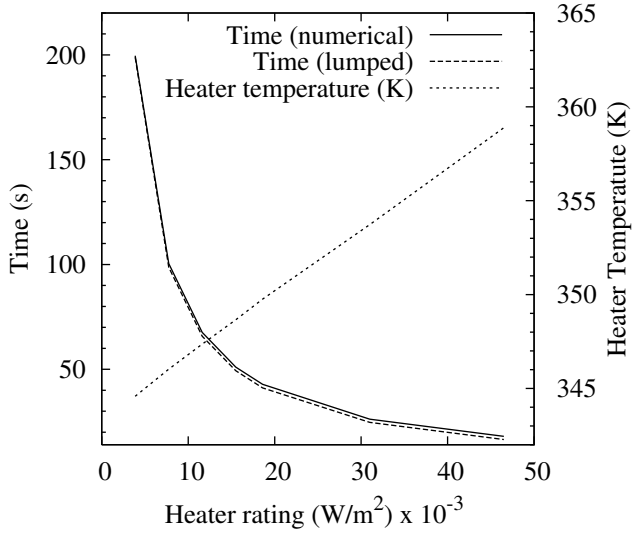

Fig. 5.6 Effect of heater Watt rating on startup time and heater temperature.

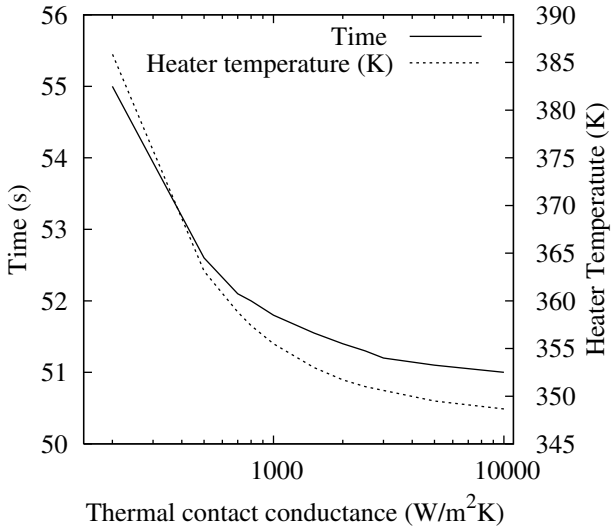

Fig. 5.7 Effect of thermal contact conductance on startup time and heater temperature. Heater rating = 15.5 x 10^3 W/m^2.

5.4.2 Using embedded wires

The key to reducing startup time is to add heat directly within the GDLs. One such technique is to embed a wire [36]. In order to analyze this heating technique, we assume the heater wires to be embedded in both GDLs as shown in Fig. 5.8. The heater wires are located at the center of the GDLs in x-y plane (see Fig 5.1). The wires extend through the length of the GDLs in the z-direction.

The wires are embedded at this location to minimize the adverse effect on the diffusion of reactants and products in the GDLs. The bare wires are chosen to have a small diameter of 25.4 μm for the same reason. The wires are insulated with a single layer

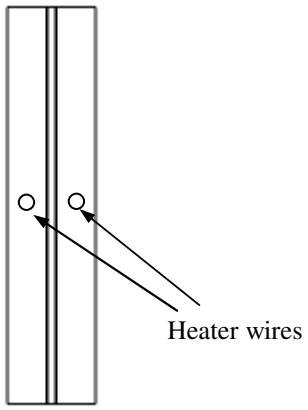

Fig. 5.8 Position of heater wires in the GDLs. The wire diameters are not drawn to scale.

of Teflon coating. The diameter of the coated wire is 30 μm approximately. In order to reduce the startup time, the wire should be made of a material that maximizes the heat generated by the wire. The heat generated by the wire for a fixed voltage electrical supply is given by

$$W = \frac{V^2}{R} \tag{5.6a}$$

where $$R = \sigma \frac{l}{A} \tag{5.6b}$$

The electrical resistivity of the wire is a function of temperature and increases with temperature. However, as the temperature of the embedded wire is expected to be below 400K, the change in the resistivity of a wire due to increasing temperature is not expected to be very large. The electrical resistance of the wire must be reduced to increase the heat generated by the wire. Copper seems to be the appropriate choice for heater wire material from that point of view. However, from a corrosion resistance point of view, other

materials like nichrome, tungsten etc. that are more commonly used for heating applications seem to be more appropriate. However, these materials have higher electrical resistivity [37]. Equation 5.6 also shows that

$$W \propto A \propto d^2 \tag{5.7}$$

Thus, wires made of materials with higher electrical resistivity and larger diameters can also provide high heat generation rates. However, the designer will also have to consider the adverse effect of larger wire diameters on reactant diffusion. Additionally, the choice of wire size will depend on the strength of the material chosen and also on the safety considerations. In this chapter we assume the heater wire to be made of copper.

The heater wire is incorporated into the Cartesian grid as shown in Fig. 5.9. The heater wire is enclosed in a square control volume with side equal to the outer diameter of the Teflon coated wire. The adjacent grid sizes are also kept small to properly resolve the temperature distribution near the wire. The heat generated by the wire is modeled as a heat generation term for the control volume containing the wire.

The GDLs in a fuel cell are made up of carbon fibers in cloth or woven form. Hence the thermal contact at the heater wire/GDL interface is not perfect. Also, the dominant resistance to heat transfer from the wire to the GDL is due to the thermal contact conductance at the GDL/wire interface. The temperature drop across the Teflon coating is very small due to its thinness. There appears to be little experimental data to predict the thermal contact conductance at this type of interface. The effect of Nusselt number (Nu_D) at the heater wire/ GDL interface on wire temperature is shown in Fig. 5.10. The minimum Nusselt number considered in Fig. 5.10 is the limiting Nusselt number for free convection over a long horizontal cylinder [38].

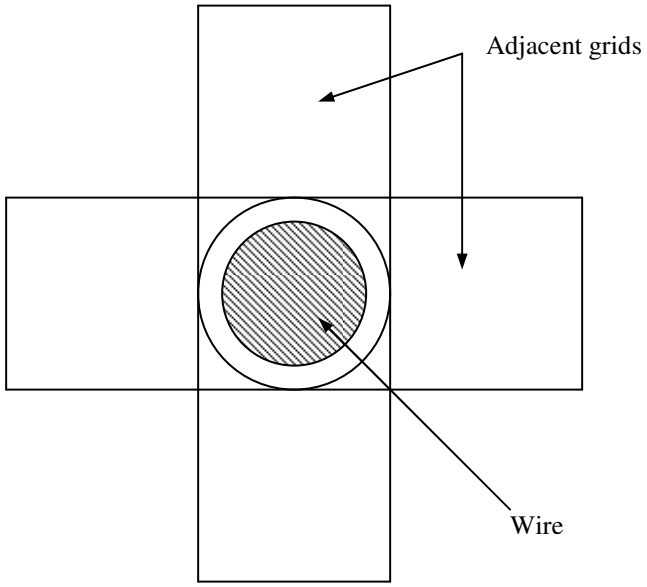

Fig. 5.9 Location of the heater wire in the Cartesian grid.

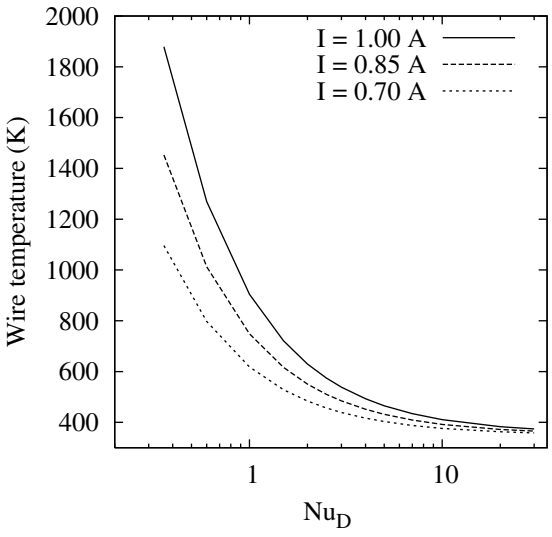

Fig. 5.10 Effect of heater wire/GDL thermal contact on wire temperature.

Air is assumed as the fluid in contact. In general, the Nusselt number at the heater wire/GDL interface can be expected to be higher due to contact with carbon fibers. Also, the properties of Teflon degrade above 533 K [39]. Additionally, in order to avoid potential premature local degradation of the GDL, the wire temperature should be kept below 400K. Figure 5.10 shows that the wire temperature decreases with increasing Nusselt number and smaller currents. Thus, an appropriate value of current should be chosen for a given Nusselt number so that the wire temperature remains well below 400K. For all the calculations shown further in this chapter, the Nusselt number at the heater wire/GDL interface is assumed to be 10.0 and the current is assumed to be 0.7 A so that the wire temperature is 376 K approximately.

It was observed that lower currents reduce the maximum MEA temperature and thus allow more uniform heating of the GDLs and MEA. However, lower currents also increase the startup time by reducing the heat generation rate. It was observed that, Nusselt number does not affect the maximum MEA temperature. This shows that the rise in the temperature of the heater wire compensates for lower Nusselt number values and the rate of heat transfer from the wire to the GDLs and MEA is not adversely affected. Nusselt number also does not affect the startup time because the heater wire has a very small thermal mass and hence the startup time is not adversely affected even if the wire temperature rises to a high value.

Figure 5.11 shows that the startup time decreases with decreasing through-plane thermal conductivity. This trend can be better analyzed using Fig. 5.12 which shows the paths for the flow of heat from the heater wires. Part of the heat generated in the wires is

used to heat the MEA and GDLs and part of the heat is transferred to the bipolar plates. The heat transferred to the gases in the gas channel is extremely small due to the low heat transfer coefficient at the GDL/gas channel boundary. Any heat transferred to the bipolar plates increases the startup time because such a heat loss reduces the heat available to heat the MEA and the GDLs. Moreover, as the thermal mass of the bipolar plates is about three orders of magnitude larger than that of the MEA and GDLs, the temperature of the bipolar plates is lower than the temperature of the GDLs and the MEA. Hence, a larger portion of the heat generated by the heater wires is transferred to the bipolar plates. Reducing the through-plane thermal conductivity reduces the rate of heat transfer to the membrane and

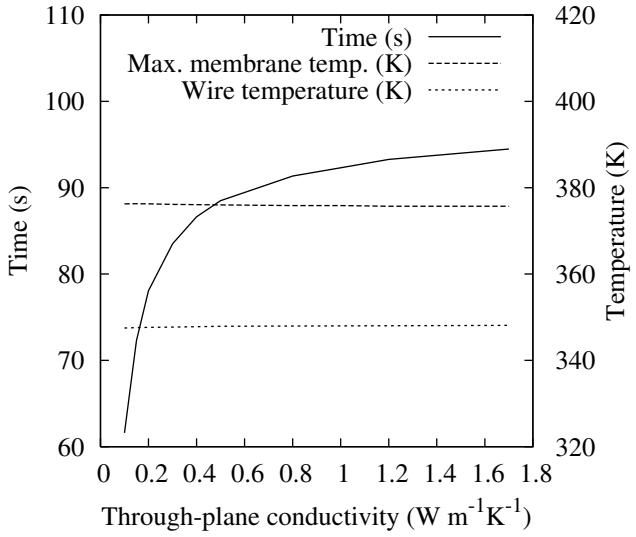

Fig. 5.11 Effect of through-plane thermal conductivity of GDL on startup time, wire temperature and maximum membrane temperature.

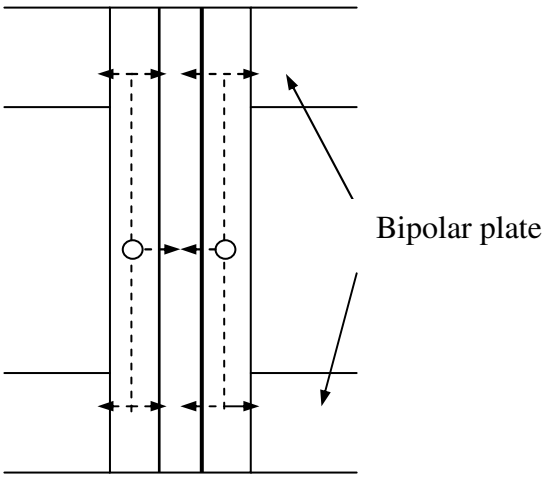

Fig. 5.12 Heat flow paths from the heater wire.

the bipolar plates. However, the reduction in heat transferred to the bipolar plates has a more significant impact and hence the startup time decreases. Figure 5.11 also shows that the startup time does not increase with higher through-plane thermal conductivity if the through-plane thermal conductivity of the GDL is greater than a certain value. At this value of the through-plane thermal conductivity, the thermal resistance in the in-plane direction becomes the dominant resistance to flow of heat from the heater wires to the bipolar plates. Therefore, any further increase in the through-plane thermal conductivity does not significantly affect the startup time. Thus, GDLs with low through-plane thermal conductivity like Teflon impregnated carbon cloth GDLs [35] can reduce the startup time for a fuel cell when used together with this heating technique. Figure 5.11 shows that lower through-plane thermal conductivity also does not lead to significantly higher wire and membrane temperatures. This is an important observation because the wire

temperature can be expected to increase as the rate of heat transfer from the wire to the bipolar plate decreases. However, as the startup time also decreases due to lower through-plane thermal conductivity, the wire temperature does not show a large increase.

Figure 5.13 shows the effect of in-plane thermal conductivity of the GDLs on the startup time, wire temperature and maximum membrane temperature. Lower in-plane thermal conductivity of the GDL reduces the rate of heat transfer from the wire to the bipolar plate and hence reduces the startup time. However, Fig. 5.13 shows that the maximum membrane temperature and the wire temperature also increase for lower in-plane thermal conductivities. Thus low in-plane thermal conductivities lead to non-uniform heating of the MEA and the GDLs and can also damage the GDLs locally due to the high wire temperatures. Thus, it is preferable to maintain the in-plane thermal conductivities of the GDL at a high value. The startup time can be decreased by lowering

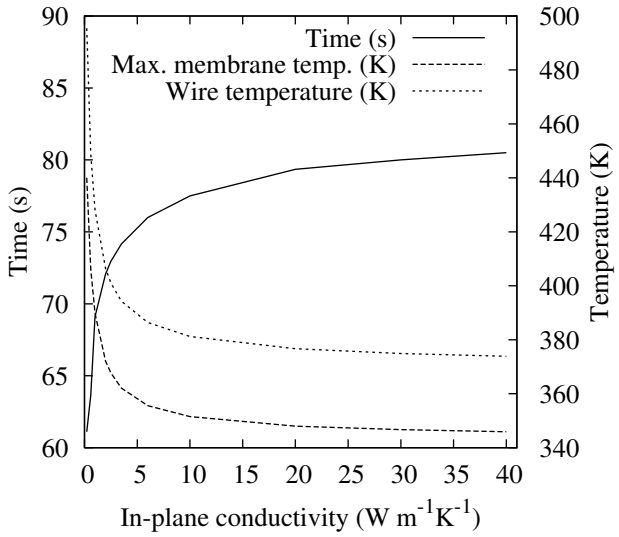

Fig. 5.13 Effect of in-plane thermal conductivity of GDL on startup time, wire temperature and maximum membrane temperature.

the through-plane thermal conductivity of the GDL as it does not adversely affect the MEA and wire temperatures.

In addition, thicker GDLs and lower thermal contact conductance at the GDL/bipolar plate interface also reduce startup time by reducing the rate of heat loss from the heater wires to the bipolar plates. However, thicker GDLs increase the resistance to diffusion of reactants and products and hence adversely affect the performance of the fuel cell. Lower thermal contact conductance at the GDL/bipolar plate interface also leads to higher temperatures inside the fuel cell. Higher temperatures can lead to membrane dehydration and may not be desirable under certain operating conditions [40].

5.5 Conclusions

The important conclusions from the study are summarized by:

1. If hot liquid is used to raise the temperature of a fuel cell, the startup time decreases with increasing flow rate of the hot liquid. Such, high flow rates for the hot liquid increase the pumping requirements for the external pump.
2. Planar, flexible heaters are better suited for fuel cell heating applications than cartridge heaters as they increase the contact conductance at the heater/bipolar plate interface and help to reduce the size of the bipolar plate.
3. If wires embedded in the GDLs are used to heat the fuel cell then the maximum allowed current in the wires is determined by the contact conductance at the GDL/heater wire interface which in turn determines the temperature of the heater wire.

4. Nusselt number at the GDL/heater wire interface affects the temperature of the wire but has a very limited impact on the startup time and membrane temperatures.
5. GDLs with low through-plane thermal conductivity and high in-plane thermal conductivity reduce startup time when used in conjunction with embedded wires to raise the temperature of the fuel cell.

5.6 References

[1] Hishinuma, Y., Chikahisa, T., Kagami, F., and Ogawa, T., 2004, *JSME International Journal, Series B: Fluids and Thermal Engineering*, vol. 47, p. 235.

[2] Yu, P. T., Gu, W., Makharia, R., Wagner, F. T. and Gasteiger, H. A., 2006, *ECS Trans.*, vol. 3, p. 797.

[3] Sundaresan, M. and Moore, R. M., 2005, *J. Power Sources*, vol. 145, p. 534.

[4] Bradean, R., Haas, H., Eggen, K., Richards, C. and Vrba, T., 2006, *ECS Trans.*, vol. 3, p. 1159.

[5] Gummalla, M., Gupta, N., Ghosh, S., Burlatsky, S., Hagans, P. and Rice, C., 2004, *AIChE Annu. Meet. Conf. Proc.*, p. 473.

[6] Sun, S., Yu, H., Hou, J., Shao, Z., Yi, B., Ming, P. and Hou, Z., 2004, *J. of Power Sources*, vol. 177, p. 137.

[7] Ge, S. and Wang, C. Y., 2007, *Electrochim. Acta*, vol. 52, p. 4825.

[8] Yan, Q., Toghiani, H., Lee, Y. W., Liang, K. and Causey, H., 2006, *J. Power Sources*, vol. 160, p. 1242.

[9] Ahluwalia, R. K. and Wang, X., 2006, *J. Power Sources*, vol. 162, p. 502.

[10] Sundaresan, M. and Moore, R. M., 2005, *Fuel Cells*, vol. 5, p. 476.

[11] McDonald, R. C., Mittelsteadt, C. K. and Thompson, E. L., 2004, *Fuel Cells*, vol. 4, p. 208.

[12] Cho, E., Ko, J. J., Ha, H. Y., Hong, S. A., Lee, K. Y., Lim, T. W. and Oh, I. H., 2004, *J. Electrochem. Soc.*, vol. 151, p. A661.

[13] Oszcipok, M., Riemann, D., Kronenwett, U., Kreideweis, M. and Zedda, M., 2005, *J. Power Sources*, vol. 145, p. 407.

[14] Oszcipok, M., Hakenjos, A., Riemann, D. and Hebling, C., 2007, *Fuel Cells*, vol. 7, p. 135.

[15] He, S., Lee, J. H. and Mench, M. M., 2007, *J. Electrochem. Soc.*, vol. 154, p. B1227.

[16] Wang, Y. and Wang, C. Y., 2007, *J. Electrochem. Soc.*, vol. 154, p. 636.

[17] Wang, Y., 2007, *J. Electrochem. Soc.*, vol. 154, p. 1041.

[18] Khandelwal M., Lee S. and Mench M. M., 2007, *J. Power Sources*, vol. 172, p. 816.

[19] Park, J. and Li, X., 2007, *J. Power Sources*, vol. 163, p. 853.

[20] Spernjak, D., Prasad, A. K. and Advani, S. G., 2007, *J. Power Sources*, vol. 170, p. 334.

[21] Lee, W. K., Shimpalee, S. and Van Zee, J. W., 2003, *J. Electrochem. Soc.*, vol. 150, p. A341.

[22] De Pillis, L.G., 1998, *Acta Applicandae Mathmaticae*, vol. 51, p. 141.

[23] Shah, R. K. and London, A. L., 1978, *Laminar Flow Forced Convection in Ducts*, Academic Press, New York.

[24] Fox, R. W. and McDonald, A. T., 2001, *Introduction to Fluid Mechanics*, John-Wiley and Sons, New York, NY.

[25] Greiner, M., 1991, *Int. J. Heat Mass Transfer*, vol. 34, p. 1383.

[26] http://www.fuelcelltechnologies.com/fuelcell/products/single_cell_hardware.asp

[27] http://www.omega.com

[28] Mikic, B. B., 1974, *Int. J. Heat Mass Transfer*, vol. 17, p. 205.

[29] http://www.omega.com/Heaters/pdf/KHR_KHLV_KH.pdf.

[30] http://www.hiheat.com/Products/Kapton-Polyimide-Heater.htm.

[31] Mirmira, S. R., Marotta, E. E., and Fletcher, L. S., 1998, *J. Thermophys. Heat Transfer*, vol. 12, p. 454.

[32] Marotta, E. E., and Fletcher, L. S., 1996, *J. Thermophys. Heat Transfer*, vol. 10, p. 334.

[33] Fuller, J. J., and Marotta, E. E., 2001, *J. Thermophys. Heat Transfer*, vol. 15, p. 228.

[34] Hollinger, A., 2006, *Contact Resistance Measurements of Gas-diffusion layers and Membrane for Fuel Cell Applications*, Senior Honors Thesis, Department of Engineering Science and Mechanics, The Pennsylvania State University, University Park, PA.

[35] Khandelwal, M. and Mench, M.M., 2006, *J. Power Sources*, vol. 161, p. 1106.

[36] Gebhardt, U. and Waidhas, M., 2000, *Fuel Cell Battery with a Heating Element and Improved Cold Start Performance and Method for Cold-Starting a Fuel Cell Battery*, abstract for WO/2000/059058.

[37] Dyos, G. T. and Farrell, T., 1992, Electrical Resistivity Handbook, IEEE materials and devices series, London, U.K.

[38] Churchill S. W. and Chu H. H. S., *Int. J. Heat Mass Transfer*, vol. 18, p. 1049.

[39] http://www2.dupont.com/Teflon_Industrial/en_US/tech_info/techinfo_com

pare.html.

[40] Bapat, C. J., and Thynell, S. T., 2007, *J. Power Sources*, article in press, available online.

Chapter 6

Summary of results and future work

6.1 Summary of results

Initially, a two-dimensional single phase model was developed to assess the importance of an anisotropic thermal conductivity of the GDLs in determining the temperature distribution inside a PEM fuel cell. The analysis shows that the thermal conductivity of GDLs can have a great impact on the temperature and its gradients inside a cell. It is desirable to have a high in-plane thermal conductivity for the GDL to generate more uniform temperature distribution inside the fuel cell. However there exists an optimum value of the in-plane thermal conductivity beyond which no significant improvement in heat transfer characteristics can be obtained simply by increasing the thermal conductivity. Additionally, anisotropic behavior of the thermal conductivity of the membrane does not have a serious impact on the cell operation. Our analysis also shows that thin GDLs do not automatically lead to lower temperatures in a fuel cell. In fact, the maximum temperatures in a fuel cell can be higher for thin GDLs than thicker GDLs if the in-plane thermal conductivity is not maintained at a high value. Also, a low value of thermal contact conductance at the GDL/current collector interface can lead to high temperatures inside the fuel cell. This contact conductance is the single most important factor controlling the temperature distribution.

In order to further improve our understanding of the fuel-cell operating behavior, we also developed a two-dimensional two-phase model to account for liquid water

generation and transport in the GDLs and catalyst layers. Using this model we were able to get additional insights into the complex interaction of various parameters affecting fuel cell behavior. We showed that the fuel cell generates high current densities with moderately high temperatures for low through-plane thermal conductivity and a high in-plane thermal conductivity of the GDL. Also, by using bipolar plates with narrow ribs and GDLs with high through-plane thermal conductivity near the inlet, membrane dehydration may be avoided for low-humidity operating conditions. Thus, the current density may be maximized at low-humidity operating conditions by tailoring the GDL to have a high through-plane thermal conductivity near the inlet and progressively decreasing the through-plane thermal conductivity at distances farther away from the inlet along the flow channel. The width of the bipolar plate ribs can also be similarly optimized to maximize the current density at low humidity inlet conditions.

We modified the two-phase model further to include the effects of an anisotropic electrical resistivity of the GDLs. We showed that while higher in-plane electrical resistivity aversely affects the local current density in the region of the catalyst layer directly exposed to the gas channel, higher through-plane electrical resistivity has a negative impact on the local current density in the entire catalyst layer. Also, the maximum and minimum temperatures in the cathode catalyst layer are determined by the average current density rather than the local current density for a GDL with highly anisotropic thermal conductivity.

We also used a three-dimensional model to evaluate different heating techniques used for startup of a fuel cell. We showed that if a hot liquid is used to raise the initial temperature of the fuel cell, then using heat transfer enhancement techniques in the liquid

channel can reduce the startup time. Also, a high flow rate within the laminar range is the optimum flow rate for hot liquid flow. We showed that, as the thermal mass of the bipolar plates is almost three orders of magnitude higher than the GDLs and MEA, using materials with lower heat capacities (like graphite, foams etc.) can reduce startup time. For the same reason, thin, flexible electric heaters are more suitable for fuel-cell heating applications than cartridge heaters. We also showed that, if heater wires embedded in the GDLs are used for fuel cell startup then the Nusselt number at the GDL/heater wire interface has to be greater then 3.5 for safe and reliable operation. Also, GDLs with low through-plane thermal conductivity and optimally high in-plane thermal conductivity reduce startup time when used in conjunction with embedded heater wires to raise the temperature of the fuel cell.

Thus, two and three dimensional numerical models were used to investigate steady state and startup behavior of a PEMFC. The analysis revealed criteria for optimizing GDL thermal conductivities to maximize the current density at different steady state operating conditions. The analysis also showed that GDL thermal conductivities can be tailored to reduce the startup time. The conclusions of our analysis will help to construct PEM fuel cells with improved operating and startup behavior.

6.2 Future work

The analysis presented here can be further improved by using more advanced numerical models and more detailed experiments. The possible improvements in model formulation and validation are now discussed.

6.2.1 Model formulation

The numerical model can be further improved by using a pore-scale model [1] instead of the macro-scale two-phase model used in this work. The pore-scale model tracks the motion of the liquid-gas interfaces through each pore of the porous medium. Even though such a model is more accurate, it requires significantly more computational power and system memory.

6.2.2 Model validation

The model results presented in this work were validated against the polarization curves because more detailed experimental data are not available in published literature. Detailed measurements of temperature and phase void fraction distributions are difficult to perform because of the thinness of the GDLs and catalyst layers. However, a combination of more detailed experiments and computational modeling can be used to generate very reliable predictions for the temperature distribution and catalyst layer liquid accumulation in the catalyst layers.

We have used the cathode reference exchange current density as fitting parameter. The cathode reference exchange current density depends on the catalyst and ionomer loading, as well as on catalyst layer porosity and thickness. Hence the reference exchange current density has to be experimentally measured for the catalyst layer under consideration. If the measurements of polarization curves are accompanied with measured values of reference exchange current densities, the cathode reference exchange density need not be used as a fitting parameter. Also, the heat generated by the fuel cell

during steady-state operation can be determined by measuring temperatures of the coolant water and reactant gases at different distances from the inlet. The concentrations of reactants at different distances for the inlet can also be measured. A computational model that incorporates measured values of exchange current densities and is validated using measurements of heat generation rates, reactant concentrations and polarization curves, can be used to generate very reliable predictions for the temperature distribution and catalyst layer liquid accumulation in a fuel cell.

6.3 References

[1] Al-Raoush and R. I., Willson, C. S., 2005, *J. Cont. Hyd.*, vol. 77, p. 67.

Appendix

This appendix provides the algorithm for the numerical scheme that is used to solve the two-phase flow equations. The model equations are given in Table 3.1. The algorithm is based on the SIMPLER scheme developed by Patankar [1] for single-phase flows. The original SIMPLER scheme was slightly modified to account for the presence of two phases. The pseudocode for the numerical algorithm is given by,

1. Set the values of all the variables to their initial conditions.
2. Update different parameter values like ionic conductivity, membrane water content etc.
3. Solve the electrochemistry equations.
4. Solve the component balance equations for concentrations of different species.
5. Solve the gas pressure equation. The gas pressure equation is derived using the sum of gas and liquid phase mass balance equations. The discretized phase momentum equations are used to express phase velocities in terms of phase pressures. The capillary pressure relationship used to express the liquid pressure in terms of the gas pressure.
6. Solve the discretized phase momentum equations for phase velocities. First order upwind scheme is used to discretize the convective term.
7. Solve the gas or liquid phase mass balance equation for phase void fractions.
8. Solve the energy equation for temperatures.
9. Find the norm of the error in solution of mass, heat and component balances.
10. If norm of error is less than the specified value

Increment the time step and go back to step 2.

Else

Go back to step 2.

11. After every 1000 time steps, check the error in steady state mass, heat and component balances.
12. If the error in steady state mass, heat and component balances is less than the specified value then steady state has been reached. Stop the program execution and write the variable and parameter values to data files.

References

[1] Patankar, S. V., 1980, *Numerical Heat Transfer and Fluid Flow*, Hemisphere, Washington, D.C.

VITA

Chaitanya Jayant Bapat

Education

Ph.D. (Mechanical Engineering)**,** The Pennsylvania State University (USA), 2008

M. S. (Mechanical Engineering), Indian Institute of Technology, Bombay (India), 2003

B. S. (Mechanical Engineering), Pune University (India), 2001

Publications

- Bapat, C. J., and Thynell, S. T., 2006, "Anisotropic Heat Conduction Effects in Proton-Exchange Membrane Fuel Cells," J. Heat Transfer, 129, 1109.
- Bapat, C. J., and Thynell, S. T., 2008, "Effect of anisotropic thermal conductivity of the GDL and current collector rib width on two-phase transport in a PEM fuel cell", J. Power Sources, 179, 240.
- Bapat, C. J., and Thynell, S. T., 2008, "Effect of anisotropic electrical resistivity of GDLs on current density and temperature distribution in a PEM fuel cell", J. Power Sources, 185, 428.
- Bapat, C. J., and Thynell, S. T., 2008, "Comparative evaluation of heating techniques for room temperature startup of a PEMFC", Sixth ASME International Fuel Cell Science, Engineering and Technology Conference, June 16-18, Denver, Colorado, USA.